2021-06

LOW-LIGHT CAMERA FIELD EVALUATION FOR UNDERWATER NIGHTTIME OPERATIONS

Moeller, Michelle L.

Monterey, CA; Naval Postgraduate School

NAVAL POSTGRADUATE SCHOOL

MONTEREY, CALIFORNIA

THESIS

LOW-LIGHT CAMERA FIELD EVALUATION FOR UNDERWATER NIGHTTIME OPERATIONS

by

Michelle L. Moeller

June 2021

Thesis Advisor:	James H. MacMahan
Second Reader:	Timothy P. Stanton

THIS PAGE INTENTIONALLY LEFT BLANK

REPORT DOCUMENTATION PAGE			*Form Approved OMB No. 0704-0188*

1. AGENCY USE ONLY *(Leave blank)*	**2. REPORT DATE** June 2021	**3. REPORT TYPE AND DATES COVERED** Master's thesis

4. TITLE AND SUBTITLE LOW-LIGHT CAMERA FIELD EVALUATION FOR UNDERWATER NIGHTTIME OPERATIONS	**5. FUNDING NUMBERS** N0001420WX01026
6. AUTHOR(S) Michelle L. Moeller	
7. PERFORMING ORGANIZATION NAME(S) AND ADDRESS(ES) Naval Postgraduate School Monterey, CA 93943-5000	**8. PERFORMING ORGANIZATION REPORT NUMBER**
9. SPONSORING / MONITORING AGENCY NAME(S) AND ADDRESS(ES) ONR (Arlington, VA 22203-1995)	**10. SPONSORING / MONITORING AGENCY REPORT NUMBER**

11. SUPPLEMENTARY NOTES The views expressed in this thesis are those of the author and do not reflect the official policy or position of the Department of Defense or the U.S. Government.

12a. DISTRIBUTION / AVAILABILITY STATEMENT Approved for public release. Distribution is unlimited.	**12b. DISTRIBUTION CODE** A

13. ABSTRACT (maximum 200 words)

A low-light, underwater, charge coupled device (CCD) video camera with a unique lens was evaluated in near-zero surface lux for operational use at night as a function of depth in the ocean. The goal is real-time video for moving underwater operations, as standard cameras need stationary long exposures and a fixed scenery. CCD video cameras handle illumination variation with pixel uniformity in low light the best. The video camera observed objects at varying distances with a filtered low-light source in a tank, validating its ability to operate at low luxes automatically. The video camera and self-contained logger were attached to a frame with Secchi disks, and a Snellen eye chart was deployed in the ocean at night (lux < 0.1). Edge detection was applied to Secchi disks in recorded images where outlines were observed to 12 m and 25 m depth in a harbor and ocean. The visual acuity is short-range and was significantly lower than night vision goggles at similar lux levels. Video results varied from the harbor with measured chlorophyll-a near 0 to 10–40 μg/L in the ocean, representing an algae bloom responsible for bioluminescence. The stirred motion of the frame induced bioluminescence that created varying effects on visibility.

14. SUBJECT TERMS low-light camera, CCD, underwater camera, object detection, edge detection, visual range, visual acuity	**15. NUMBER OF PAGES** 73
	16. PRICE CODE

17. SECURITY CLASSIFICATION OF REPORT	**18. SECURITY CLASSIFICATION OF THIS PAGE**	**19. SECURITY CLASSIFICATION OF ABSTRACT**	**20. LIMITATION OF ABSTRACT**
Unclassified	Unclassified	Unclassified	UU

NSN 7540-01-280-5500

Standard Form 298 (Rev. 2-89)
Prescribed by ANSI Std. 239-18

THIS PAGE INTENTIONALLY LEFT BLANK

Approved for public release. Distribution is unlimited.

LOW-LIGHT CAMERA FIELD EVALUATION FOR UNDERWATER NIGHTTIME OPERATIONS

Michelle L. Moeller
Lieutenant Commander, United States Navy
BS, U.S. Naval Academy, 2010

Submitted in partial fulfillment of the
requirements for the degree of

MASTER OF SCIENCE IN METEOROLOGY AND PHYSICAL OCEANOGRAPHY

from the

NAVAL POSTGRADUATE SCHOOL
June 2021

Approved by: James H. MacMahan
Advisor

Timothy P. Stanton
Second Reader

Peter C. Chu
Chair, Department of Oceanography

THIS PAGE INTENTIONALLY LEFT BLANK

ABSTRACT

A low-light, underwater, charge coupled device (CCD) video camera with a unique lens was evaluated in near-zero surface lux for operational use at night as a function of depth in the ocean. The goal is real-time video for moving underwater operations, as standard cameras need stationary long exposures and a fixed scenery. CCD video cameras handle illumination variation with pixel uniformity in low light the best. The video camera observed objects at varying distances with a filtered low-light source in a tank, validating its ability to operate at low luxes automatically. The video camera and self-contained logger were attached to a frame with Secchi disks, and a Snellen eye chart was deployed in the ocean at night (lux < 0.1). Edge detection was applied to Secchi disks in recorded images where outlines were observed to 12 m and 25 m depth in a harbor and ocean. The visual acuity is short-range and was significantly lower than night vision goggles at similar lux levels. Video results varied from the harbor with measured chlorophyll-a near 0 to 10–40 μg/L in the ocean, representing an algae bloom responsible for bioluminescence. The stirred motion of the frame induced bioluminescence that created varying effects on visibility.

THIS PAGE INTENTIONALLY LEFT BLANK

TABLE OF CONTENTS

THIS PAGE INTENTIONALLY LEFT BLANK

LIST OF FIGURES

LIST OF ACRONYMS AND ABBREVIATIONS

CCD	charge coupled device
CDOM	colored dissolved organic matter
Chl_a	chlorophyll-a
CMOS	complementary metal-oxide-semiconductor
COVID-19	Coronavirus
IOP	inherent optical properties
MTF	modulation transfer function
ND	neutral density
NTU	nephelometric turbidity units
NVG	night vision goggles
OD	optical density
UW	underwater
VR	visual range
VTF	visual threshold function

THIS PAGE INTENTIONALLY LEFT BLANK

ACKNOWLEDGMENTS

I would like to thank Jamie MacMahan for guiding me through every aspect of this process. It has not been an easy time trying to navigate field research amidst the pandemic, but Jamie made sure I had everything I needed to compile a thesis I could be proud of and managed to keep me laughing along the way. It has been an extremely rewarding experience I will never forget. Additional thanks to Paul Jessen, Keith Wykoff, Mike Cook, Tim Stanton, Miguel Green, Charlotte Benbow, and the countless others from the Naval Postgraduate School Meteorology and Oceanography Department faculty and staff. Special thanks to my cohort for always being there to lend a helping hand and working as a team to get through a challenging couple of years. I would also like to thank my family, those near and far, for their endless support throughout this process.

THIS PAGE INTENTIONALLY LEFT BLANK

I. INTRODUCTION

The human eye is uniquely developed to see in both day and night. The central clock system in humans links to geophysical time via various photic cues perceived by the retina (Dibner et al. 2010). The sun is the most critical source of these photic cues, and at nighttime, this includes the illumination provided by its reflection off the moon. The human eye retina is lined with multiple types of cells, photoreceptors, that respond to different light types. The cells that process most light are called cones (Yamakawa et al. 2019). The cone photoreceptors provide humans with high levels of visual acuity, or sharpness, and are split into categories based on peak sensitivity, roughly 565 nm, 530 nm, and 430 nm, allowing color recognition (Danilenko et al. 2009). The cones are ultimately responsible for vision throughout the daylight hours, also known as the photopic domain. In contrast, the rods lack the visual acuity of the cones and are responsible for human sight at night. A single rod is present in humans with a peak sensitivity at 496 nm (Danilenko et al. 2009). The single peak heavily reduces the ability to see color and is primarily described as black and white. Human night vision is limited to the scotopic domain, reduced sharpness, and no color.

Even in direct sunlight, acceptable conditions for underwater visibility in the ocean decrease at an exponential rate with depth. Light will interact with water molecules immediately upon entering the sea, and a diverse range of materials will have massive impacts on the depth light can reach (Dickey et al. 2011). The euphotic zone is defined as roughly 2.5 times the Secchi disk depth, usually extending to no more than 50-100 m (Strickland 1958). Within this zone, the vertical distribution of phytoplankton can also play a significant role in reduced visibility since it is heavily reliant on light penetration (Batistić et al. 2012). Moving into the disphotic zone and beyond (~200 m and more), extremely low light intensities exist, resulting in one of the world's darkest habitats. Faint ambient light is provided through bioluminescence, but it tends to be intermittent (de Busserolles and Marshall 2017). Creatures such as the giant and colossal deep squid are amongst the mesopelagic organisms that have developed enhanced visual systems to operate in this harsh low-light environment.

The giant and colossal deep-sea squid lurk at depths more than 1000 m, with eyes spanning greater than 25 cm in diameter. Their eyes, roughly three times the size of any other animal, did not evolve in such a way to find mates or food but rather as a means of protection (Nilsson et al. 2012). The giant squid can see distances greater than 100 m in a highly harsh visual environment, at depths where bioluminescence takes over as the primary source of light well beyond where sunlight can penetrate (Widder 2002). The visual capabilities of these deep-sea creatures extend far beyond the low-light capabilities of the human eye. Humans must rely on various forms of low-light technology to close the gap.

Human vision can be enhanced with technology at low-light levels, measured in lux, representing lumens per area. Night vision goggles (NVGs) are commonly known to enhance humans' ability to see and operate in low-light conditions on land (Parush et al. 2011). Though widely used in military operations, NVGs have a strong reputation for aiding in low-light object detection. Still, they are not necessarily praised for their high-resolution images compared to a camera phone or standard video camera. NVGs are image intensifiers that amplify ambient light and project the image onto a phosphor screen (Revell and Hignett 2004). It was difficult to ascertain an exact number for the lowest lux levels that a human can detect, but it is safe to say that human vision and NVGs overlap in their low-light detection levels. Even though humans may see these low-light levels, it does not mean that they can safely operate or do so with any sense of urgency. NVGs allow full-speed operations in the dimmest conditions. Recent generations of NVGs have demonstrated impressive growth in at least one of the critical areas of gain, noise, spectral sensitivity, resolution, or the more physical categories of size, weight, and ruggedness (Pinkus and Task 1998). Still, even NVGs have a lower light limit where the image becomes too noisy for operational use.

When researching for the right technology to meet low-light requirements, it was essential to consider baseline exposure factors like the aperture and shutter speed required to produce a usable product (Torres and Menéndez 2015). Aperture is the opening that limits the amount of light that reaches the sensor, and shutter speed controls the length of time the sensor is exposed to the light. In low-light environments, there are a couple of

options to overcome exposure shortcomings. One option is to set a longer exposure time (slow shutter speed) to give the camera enough time to collect all available light to produce an image. Slow shutter speed is beneficial only when there is no movement of the camera or scene. Unfortunately, this approach eliminates the ability to evaluate in real-time. A second option is to widen the aperture for more light. The negative here is that it heavily decreases the depth of field, only allowing for focus of nearby targets (Petschnigg et al. 2004). In the end, to operate in a low-light environment with a constantly evolving scenery and moving camera, a combination of the correct aperture and shutter speed must be met. The best way to accomplish this is through video cameras specializing in automatic adjustments to prevent over-saturation at higher light levels and provide the best chance at a viable image in low-light.

Images obtained by video cameras that operate in the lowest regions of the visible spectrum and near IR, like charge-coupled devices (CCDs) or complementary metal-oxide-semiconductor (CMOS) imagers, are required to cope with variation in illumination seamlessly (Huber et al. 2002). When identifying a correct imager, CCD, or CMOS, it is essential to consider several attributes that affect the quality of the image being produced and the complexity and cost of the system. Historically, CCD cameras were considered the low-light premier imager primarily due to uniformity or the consistency of various pixels in identical illumination conditions. Ideally, a consumer is looking for a uniform response across all pixels. In typical CMOS imagers, since each pixel is responsible for its electron to voltage conversion, this leaves room for discontinuities and variation. There is only one electron voltage conversion in CCD imagers for all pixels at an output node (Litwiller 2005). There was a more uniform image in CCDs and significant dark nonuniformities in basic CMOS imagers. For most CMOS imagers, they could offer better integration, an extended battery life, and a smaller size, but this was almost always at the cost of image quality (Litwiller 2001).

CMOS imagers have made impressive strides in recent years, closing the gap in categories like the low-light environment that was once solely dominated by CCDs. The Canon ME20F-SH, featuring a new high sensitivity CMOS, is one such example. Canon's premier technology boasts two innovations in CMOS image sensors. The first is a new 35

mm CMOS image sensor specifically developed to support high dynamic range (Thorpe 2016). The second plays on the large 35mm full-frame CMOS image sensor with an enhanced spatial sampling to realize a uniquely large photosite (Thorpe 2016). These advancements allow for unprecedented low-light sensitivity suitable for deep underwater imaging with no additional light required (Thorpe 2016). More specifically, the Canon features a 2.2MP high sensitivity CMOS. It offers full-color video in extreme low-light conditions claiming a minimum subject illumination of 5×10^{-4} lux, at a maximum 75 dB gain (Canon 2015). Although appealing in capability, Canon charges around $20,000 for the baseline and requires additional purchases such as appropriate lenses and underwater housing.

For a fraction of the price and a more impressive low-light sensitivity, the Teledyne Bowtech Explorer Pro video camera comes already optimized for underwater low-light operations. It is an adapted CCD sensor coupled to a wide-angle, high speed, aspherical auto-iris lens made of fully water corrected quartz glass. The faceplate of the video camera allows a low-light sensitivity of 2×10^{-5} lux, an order of magnitude more sensitive than the Canon. The video camera can reach depths up to 2000 m, but realistically, object detection and visibility are limited to much shallower depths and distances with no artificial light source (Teledyne Bowtech Ltd 2020).

Ocean visibility and underwater object detection are challenging. Particulate matter like colored dissolved organic matter (CDOM), chlorophyll, or other types of debris within the water column can heavily impact visibility, causing reduced ranges as low as a few cm in murky waters (Dickey et al., 2011). According to Dickey, Kattawar, and Voss (2011), when viewing larger targets in the ocean, there is a reduction in contrast as ambient light scatters, making detection increasingly tricky. With a smaller target or the same target at a farther distance, reflected light from the target could also hinder contrast, causing images to appear blurry (Dickey et al., 2011). A blurred object may be better than nothing, but it is vital to recognize a blur of an object as different from the fine details of an object. Object detection in water is not easily quantifiable and only remains complex when coupled with a low-light environment. Assessing the visual acuity of the selected video camera with an adapted Snellen eye chart provided additional data points and more advanced results.

Visual acuity is a measurement of the eye's ability to resolve fine detail and is the standard assessment of visual function common in eye examinations (Attebo et al. 1996). The basis of acuity is that the letter width (that also describes the letter height) ω, is defined by

$$w = 2d \tan\left(\frac{\theta}{2}\right) \quad [1]$$

d is the observer's distance from the eye chart, and θ is the angle subtended by the letter in degrees based on 5 arcminutes specified by Snellen (Howett 1983). Eq. [1] is based on the letter width that represents the line for 6 m/6 m acuity. For example, based on d=6 m, the letter P will be 8.73 mm tall for 6 m/6 m acuity. For 6 m/60 m acuity, the letter P would be 87.3 mm tall. The letter P is ten times larger, representing a distance that is 10 times farther. As suggested by countless NVG studies, the assessment of visual acuity provides direct insight to object detection and visibility within attempts to validate the Teledyne Bowtech Explorer Pro video camera for future military operations.

Numerous factors played into the decision to pursue testing with the Teledyne Bowtech Explorer Pro video camera to accomplish the overarching goal of underwater object detection in the low-light environment. The simplicity provided by the auto-iris and auto dynamic range allowed deployments without the constant fear of incorrect settings. The minimum illumination was an order of magnitude less than the Canon. Even with the required electronic housing and frame, the size was still manageable for a single person. It did not require a separate housing or lens purchased for underwater use and cost ~10 times less than the Canon plus housing. A couple of negatives were that it is not commercially available. Primary settings cannot be adjusted without professional assistance. The system required an external logger to be configured to capture data from the video camera.

The first goal of this project was to create a system that allowed the video camera to log the video images it was acquiring within the low-light environments. This system required a compatible data logger, a battery to power both the logger and video camera and underwater housing to protect all electronics. After the power and logging were operational, a frame to mount the video camera, electronic housing, and provide targets

within the video camera's field of view needed to be assembled and tested. Once an operational frame was built, it needed to be tested, and finally, the resultant images were required to be evaluated for accurate object detection. The ultimate goal is to validate the Teledyne Bowtech Explorer Pro video camera as a low-light underwater camera that can provide precise object detection at depths >20 m under natural surface illumination conditions.

II. METHODS

A. AN OVERVIEW OF METHODS AND PERTINENT ISSUES THAT INFLUENCED THE METHODS

The methods for evaluating the Teledyne Bowtech Explorer Pro, from here on referred to as video camera, were strongly influenced by the Coronavirus (COVID-19), as this closed the school and facilities, induced purchasing and shipping delays, and required physical restrictions. The original plans were forced to be revised or canceled altogether. The methods outlined below were designed to recognize these new limitations while maintaining progress in the project. Besides, the video camera had the wrong initial setting issues, which caused further modifications.

There were a few issues with the video camera. There was a 6-month delay in receiving the video camera, materials, logger, and batteries owing to COVID-19. Open ocean testing did not begin until October to November 2020 until COVID-19 restrictions were lifted for a small boat operation. These field tests revealed that the video camera was incorrectly configured for low-light operations. In early December 2020, the video camera was returned to its parent company. The video camera settings were not set to the lowest dynamic range of the video camera. However, the news was positive. The incorrect setting induced about a 4-month delay.

A series of garage experiments were performed in COVID-19 isolation to evaluate off-the-shelf cameras using long exposure times while the video camera was being corrected. The project goal is instantaneous images that are only achievable through video. The long exposure times highlight the difficulty that the video camera needs to overcome to provide usable images.

A series of laboratory tank experiments were executed owing to the logistical constraints and more conservative approach to evaluating the video camera upon its return. The experiments provided a more controlled setting performed with reduced personnel that was independent of the field conditions. As will be shown, the tank experiments proved that the new video camera settings worked very well.

Based on the success of the tank experiments, new evaluations moved quickly back into the field. The field experiments first took advantage of the Monterey harbor docks and low background harbor lights for the initial field validation. Small boat deployments followed additional experiments to obtain measurements farther away from artificial light sources and deeper depths.

Here the methods are described based on the constraints stated above, starting with the stationary camera phone garage experiment to evaluate the exposure time required for visibility (Section IIB). Section IIC discusses the Teledyne system's underwater assembly, including the connection to and contents of the housing and the frame setup of the video camera, underwater housing, and Secchi disk targets that provided a platform for all field deployments. Next, the controlled lab experiment validated the video camera as a functional low-light camera post-reconfiguration (Section IID). The field methods (Section IIE) begin with the Monterey harbor vertical casts to test for basic object detection with depth in the horizontal look orientation. The final methods section is the open ocean vertical casts (Section IIF), once again in the horizontal look orientation, to evaluate extreme low-light object detection and visual acuity up to 40m.

B. CAMERA EVALUATION/EXPOSURE TIME

A series of low-light tests were first performed on land with a readily available camera, the Galaxy Note20 Ultra (camera phone), to manage expectations for future low-light underwater deployments. The camera phone operates with a 108-megapixel primary sensor that dynamically shifts to a 12-megapixel image with nona binning algorithm (Idrees 2020). In simple terms, in its low-light setting, it combines data from a larger number of pixels into one larger pixel with more light. The experiment was performed in a blacked-out room. One candle, equivalent to approximately 10.76 lux, was the light source and the back wall, with flags of different patterns, words, and colors, served as the target seen in Figure 1. The camera phone remained stationary at 5.8m from the wall, and the candle was placed at three distances of 2.74 m, 1.52 m, and just below the camera phone. Camera settings of ISO 3200 and aperture 1.8 remained consistent, and the shutter speed was adjusted after every image from 1/15 s up to 30 s to allow for varying exposure

levels. This experiment describes an ordinary camera phone's performance in low-light conditions and sets expectations for an advanced low-light camera.

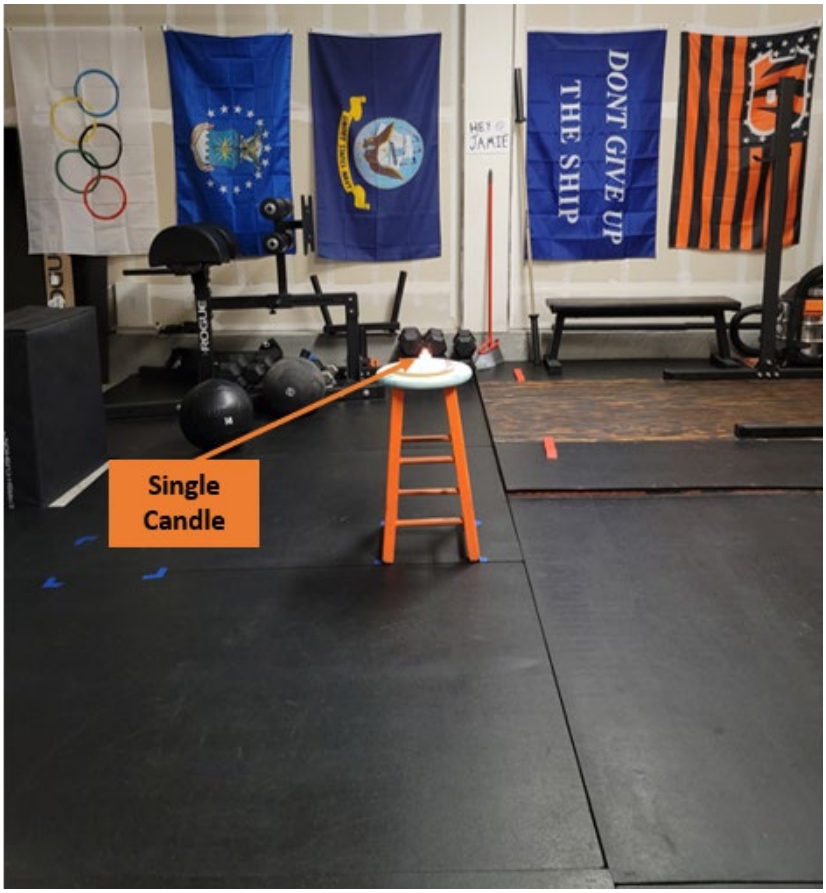

Low-light land experimental setup before the blackout. Image captured by the stationary Galaxy Note20 Ultra 2.74 m from the candle and 5.8 m from the back wall.

Figure 1. Low-light garage experimental setup.

C. TELEDYNE BOWTECH EXPLORER PRO VIDEO CAMERA, UNDERWATER LOGGER, AND OBSERVING FRAME

The underwater Teledyne Bowtech Explorer Pro video camera is a black and white CCD video camera enhanced with a unique lens to operate to a minimum sensitivity of 2×10^{-5} lux (Teledyne Bowtech Ltd 2020). The video camera has no direct logging capabilities nor an internal battery. It supports an underwater connector for power and video output. The goal is to analyze video after deployments. A separate underwater

canister (Ocean Innovations) was required that housed a rechargeable battery (12 Vdc 50 Wh Li-Ion) and video data logger (Talitor HVR-D1) for viewing and recording (Figure 2a). The battery selected herein provides >10 hrs of power to the video camera, logger, and optional external AV monitor. The logger stores the AVI-formatted video onto a standard removable SD card. The underwater battery/logger housing supports underwater connectors and cables that connect to the video camera. An additional underwater connector is available for an external monitor. The external monitor is used for pre- and post-deployments to ensure that the video camera and logger work correctly. The continuous use of the external monitor was not appropriate during field deployments for 1) the monitor produces a significant amount of artificial light source, and 2) the cost and complexity of an underwater video cable that would extend to 40 m water depths. The system power switch is a twisting red power knob (e.g., clockwise direction for on). A secondary magnetic switch enabled video logging because the logger remote could not wirelessly penetrate the canister housing. When the magnet is against the housing, the system is logging (Figure 2b-c).

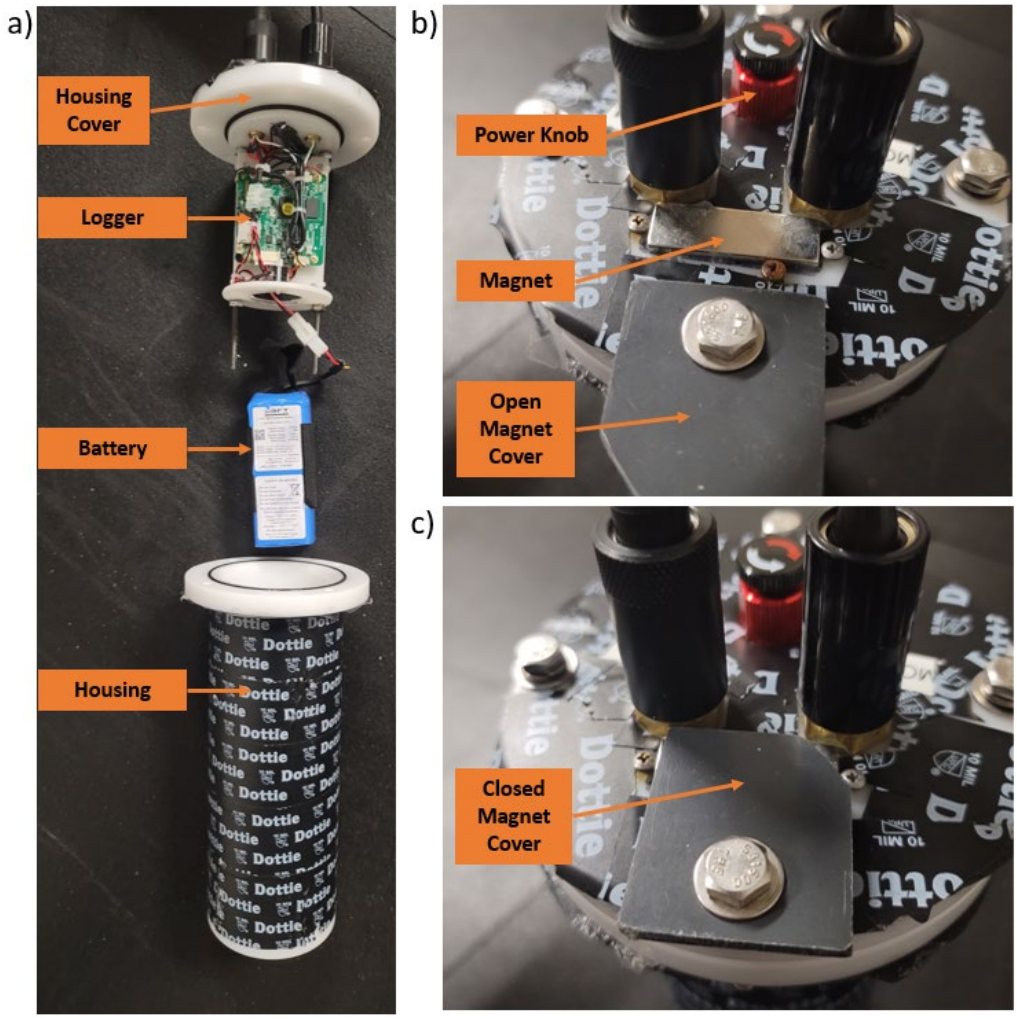

(a) Configuration of data logger and battery within underwater electronics housing. (b) The red power knob turns clockwise to supply power to the video camera and logger. Magnet set into place to start recording. (e) Magnet is secured for deployment.

Figure 2. Electronics housing.

A lightweight, rigid frame was designed for performing vertical casts through the water column by a human to obtain video images as a function of depth. The goals of the frame were to ensure that targets always remained in the video camera's field of view when deployed in the presence of ocean currents and waves. A 2.5 m long aluminum frame secures the video camera and power/logger housing on one end and connects visual targets at varying distances from the video camera (Figure 3a-b). The maximum image distance is limited to 2.0 m once the video camera is secured, which was deemed reasonable based on the video camera pixel resolution, fisheye distortion of the lens, and suggested operational

needs. The frame weighs approximately 13 kg and is deployable by one person. The targets are 20 cm black-and-white Secchi disks and can be placed anywhere from 0.5-2.0 m from the video camera. Three independent targets were found as the limit to avoid overlap in the video camera's field of view, where two of the targets were mounted on extended arms. With three targets, there are some limitations on distances to avoid target overlap. The frame can be deployed vertically or horizontally to provide different look angles relative to the surface light.

An RBR Solo D pressure sensor mounted to the frame with a pressure transducer collocated at the video camera lens provides water depth for the vertical casts. Since the video logger and pressure sensor are independent systems, their clocks are time-synced before each experiment.

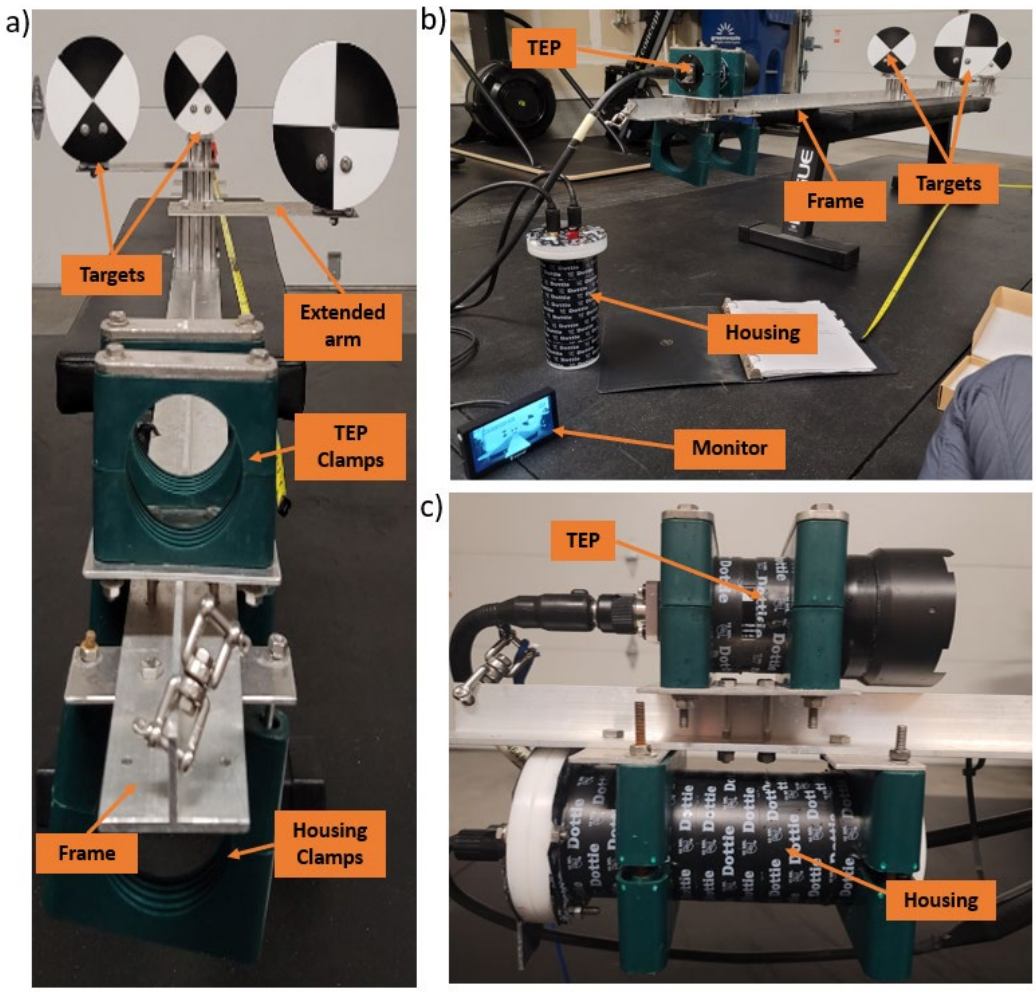

(a) Frame with adjustable Secchi disk targets and green clamps secure the camera on top and electronic housing on the bottom. (b) A pre-deployment test of the system using a standard AV monitor. Post-test, the monitor cable is replaced with a dummy plug, and the housing is secured in the green clamps below the video camera. (c) Video camera and electronics housing when secured on frame.

Figure 3. Deployable frame setup.

Inherent optical properties (IOPs) of the water column are defined by the particulates (sediment, bubbles, amongst others), biota, and dissolved organic matter in the ocean (Pegau et al. 1999) and will determine the amount of light transmission from the surface and the visibility of objects in the water. An RBR Maestro multi-channel logger was deployed at the exact locations of the video camera casts. The RBR Maestro was placed in a metal cage for protection and slowly lowered from the pier or boat to the desired depth or seafloor. It was deployed separately from the frame casts due to optical lights that

sensors produce to measure the IOPs. A sampling rate of 2 Hz provided conductivity, temperature, pressure, CDOM, chlorophyll-a (chl_a), turbidity, depth, and salinity. The three optical measurements (CDOM, chl_a, and turbidity) provide a bulk estimate of the IOPs for Monterey Bay. More sophisticated measures are required for the full IOP water column description, such as using a Wetlabs AC-S. The full IOP description was beyond the scope of the project's initial goals but would be valuable for future experiments. The IOPs are properties of the water column that do not depend on the available light. Knowing the IOPs of the water column can explain varying ranges as seen by the video camera and provide a more accurate estimate of the visual range as a function of depth quantified by the Hydrolight model (Mobley and Sundman 2001).

The video camera operates at lux levels that are well under all commercially available lux meters. In reality, the video camera is the best measure of low lux, but it is not designed to estimate lux. To date, the best estimates of lux can only be obtained through the Hydrolight model, which has performed well in daytime conditions (Stephany et al. 2000).

D. LABORATORY TANK EXPERIMENT

The video camera is designed with its unique lens to operate correctly in an underwater setting. A laboratory tank experiment provided a controlled underwater approach to testing the video camera in low-light. A tank is a conservative approach implemented as a simple, convenient pre-test to perform a fundamental evaluation. The underwater laboratory experiments were performed in an existing large (1.80 m x 0.61 m x 0.61 m) tank with a controlled low-light environment to evaluate the video camera (Figure M41b). The location of the tank required multiple controls to eliminate external light sources. The entire room required blacking out windows, taping cracks through doors, and covering small lights on computers and equipment. All experiments were performed at night to further reduce slight transparencies in the black window covers. Hallway lights were also turned off. A 0 lux environment was created, and nothing could be seen in the room when the lights were off.

The tank was set up with the video camera at one end and targets with adjustable distances and heights from the video camera located downrange. The square (7.62 cm x 7.62 cm) targets were attached via Velcro to vertical PVC poles anchored into pre-drilled holes along three 2x4s weighted to the bottom of the tank (Figure 4a). The tank supported up to three simultaneous targets. The targets were painted eggshell white with 80% reflectibility. Black letters ranging from 0.63-5 cm in height were written on the targets to test visibility beyond target detection (Figure 4c). All remaining materials were painted matte black to prevent reflection or affect the video camera's ability to identify the targets. The external video monitor was connected and located under a dark, multi-layered blanket for the laboratory tests. An initial evaluation of the video camera was performed, and video images were evaluated afterward. Upon the initial viewing of the targets, it was found that the video camera was working well at low-light levels. Therefore, the targets were turned 180 degrees to see if the video camera could identify finer details such as the back PVC pole or black Velcro. The experiment focused on distances of 21-81 cm, representing the approximate length of the human arm to perform operations with the notion that the video camera was located on an operator's shoulder. The filling hose along the back of the tank and the bottom slotted boards provided additional information in the images (Figure 4c).

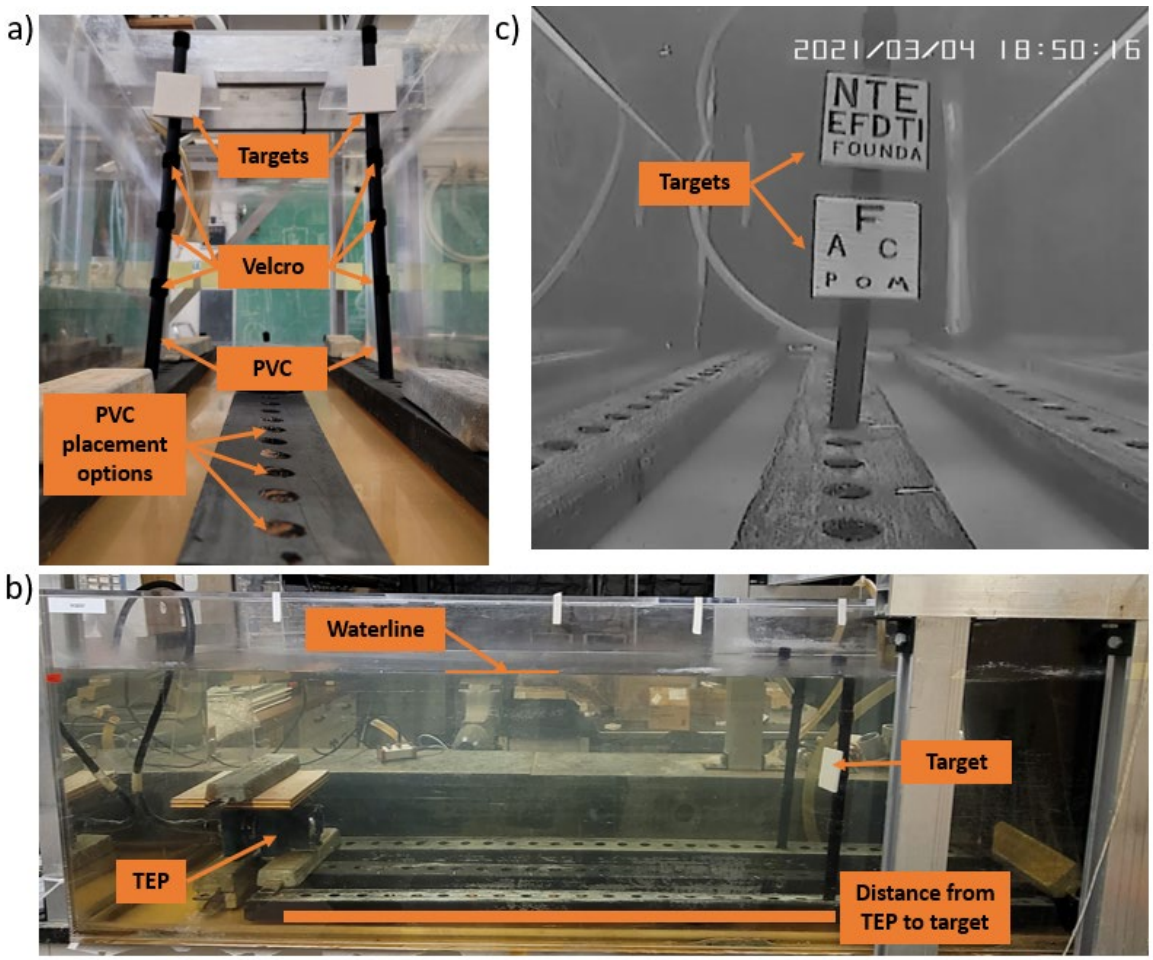

(a) Pre-experimental tank setup. Options for PVC placement can be seen drilled into the 2x4s in the bottom half of the image, and the Velcro notches along the PVC pipe allow for changes in target height. Weights ensured 2x4s remained stationary and were removed from FOV before testing. (b) video camera set up in the lower left of the image. The tank was filled with water, and targets were placed at various distances downrange. (c) Sample image captured from the video camera.

Figure 4. Lab experimental setup.

The primary light source was an underwater diving light (UW light) attached in line with the video camera inside the tank providing 75 lumens. The UW lux was adjusted by a series of neutral density reflective filters (ND filters) (Figure 5a) for a range of optical densities (ODs), providing a light transmission percentage ranging from 0.01% to 79%. These were placed over the UW light to attain low-light conditions less than those achieved from the minimum power output of the UW light (Figure 5c). To ensure all light was

focused through the filter, a washer was fixed to the faceplate of the UW light to narrow the beam (Figure 5b)

The optical densities relate to the nominal light transmission as provided by THOR labs. Initial testing of the filters with a light source and the EXTECH EA30 light meter (Figure 5d) revealed all filters to be within one percentage point of the listed nominal light transmission, except for OD 0.3, which tested around 4% higher. The filters could be stacked to further reduce lux to those in the close range of the video camera.

(a) ND 4.0 reflective filter can be attached to the UW light to reach lux levels below its minimum limit. (b) Diving flashlight with washer cover to focus beamwidth within filter size limitations. (c) UW light with ND filter attached. (d) EXTECH lux meter.

Figure 5. Underwater light, neutral density filter, and lux meter.

Attempts were made to calculate the lux as a function of distance for the 75 lumen UW light. The lux calculation proved difficult. An estimate of the beam diameter is required to describe the beam's cross-sectional area to convert lumens to lux (Figure 6a). The beam's outer edge was blurry, making measurements of beam diameter difficult. Furthermore, the light appeared to have a slight halo, further complicating estimates. Lastly, these measurements were made in the air, not water, and thus could not account for the higher light attenuation in water. Though a general trend appeared reasonable, the number of errors for lux at this sensitivity was considered too large and not provided. Furthermore, in the end, the tank was a first-order test to determine if the video camera would work at low lux levels, which it did. A primary project goal is to utilize natural light or more homogeneous light sources.

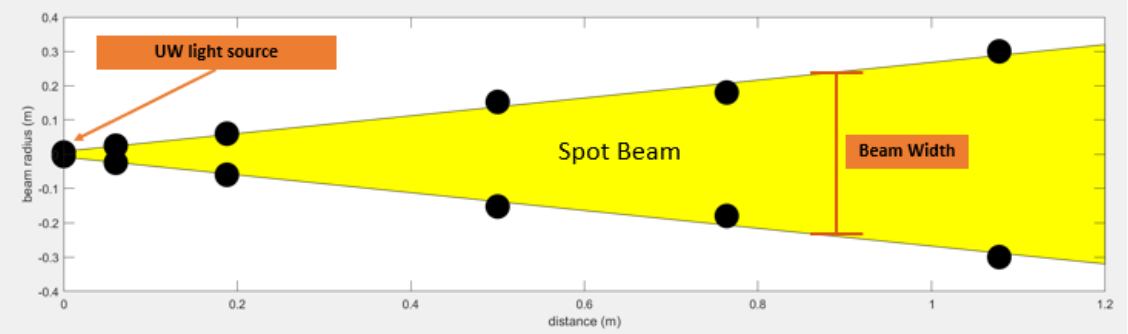

Example of the spot beam produced by the UW light source. The black dots represent the outer boundaries of the beam width diameter measured at a certain distance, and the yellow represents the spreading of the beam width with distance. As distance increases, lux level will spread and, as a result, decrease at any point.

Figure 6. Beam produced by the underwater light source.

E. MONTEREY HARBOR VERTICAL CASTS

Harbors provide a unique scenario for evaluating the video camera in the field with natural ocean waters and at night. The docks and piers extend to varying water depths that are easily accessed by foot. The light sources from streetlights, boat lights, and lights along the docks are relatively low and constant. The different configurations of the docks and piers allow for different surface lux levels.

Collocated vertical measures of the video camera and IOPs were obtained at 5 locations along the Breakwater Cove Marina docks and the Municipal Wharf #2 in Monterey Harbor well after sunset on March 24, 2021 (Figure 7). The deployment depths ranged from 4-12 m. The surface lux measured before each frame cast ranged from 0.11 for 4 casts to 26.97 lux directly under a harbor streetlight. It was a cloudless night, and the moon was at 83.8% illumination. The maximum possible photopic illuminance of the moon at approximately 0.3 lux would put us at a full estimated background lux of 0.251 lux. The frame was set up in a horizontal look orientation. Video logging sampled at 2 Hz. The frame was lowered and raised at about 35 cm/s until the frame hit bottom, where the frame rested for approximately 10 s. Separate IOP casts were performed at a similar speed.

After sunset in Monterey Bay, CA, locations of the five horizontal casts were performed on March 24, 2021. The first four casts took place at Breakwater Cove Marina, and the final cast took place at Municipal Wharf 2.

Figure 7. Monterey harbor cast locations.

The human brain is a fantastic computer and filter, which creates inherent biases. Image edge detection techniques provide an alternate unbiased approach to determining if objects or shapes in the image can be recognized. Edge detection techniques are available as part of the MATLAB image processing toolbox supported by the Naval Postgraduate School. The edge detection feature locates object boundaries and provides a binary output where 1 is the edge associated with sharp gradients (discontinuities) in image brightness, and 0 is considered the homogeneous portion of the image (MathWorks 2021). Here, edge detection was applied to the Secchi disks in the initial deployments and the lettering on the

last deployment's eye chart. Edge detection provided quantity for visual recognition as a function of depth or lux level.

F. OPEN OCEAN VERTICAL CASTS

Three separate open-ocean deployments were performed from a small boat in Monterey Bay for two reasons. First, obtain measurements under natural light, away from artificial light that occurred with the harbor deployments. Second, the success of the harbor vertical casts showed that the lower lux limit of the video camera required deeper depths. The first two deployments were simple assessments of the video camera and exploring the fundamental question of "Does the video camera identify the three Secchi disks in a deeper, lower lux scenario?" Based on the success of the two deployments, the final deployment aimed toward a more critical assessment of visual acuity.

The first deployment occurred after sunset on November 16, 2020, where it was discovered that the video camera was not configured properly for low-light conditions. The video camera was returned to its parent company and re-configured with the appropriate settings. The second deployment, location provided in Figure 8, occurred on the full moon night of March 29, 2021, with the same settings (sampling rate, look orientation, and Secchi distances) and process as the harbor tests: a lux reading and a slow horizontal frame cast (35 cm/s), and a separate IOP cast. The frame was lowered to approximately 27 m and did not reach the ocean floor before retrieval. There was only one cast on the 29th due to high seas (3 m height with 9 s period) that caused violent jolts throughout the cast.

The open ocean deployments in Monterey Bay, CA, are located on March 29 and April 16, 2021. The green line indicates the 25 m isobath. The depth of the cast on March 29 was ~30 m, and the depth of the cast on April 16 was ~40 m.

Figure 8. Monterey Bay open ocean deployment locations.

The final deployment, the location provided in Figure 8, occurred on April 16, 2021. Results from the harbor tests influenced the methods for the last deployment attempting to dig deeper into quantifying object visibility. Unlike the previous deployment that took place just after sunset around 2000, the April 16 deployment began at 0400 to ensure complete darkness from start to end and calmer winds and seas. The cast also included a 10 s pause every 5 m on the upcast to allow the video camera additional time to focus. The moon was at 20% illumination, and two casts were lowered to a depth of 40m. Similar deployment procedures were in place for the casts; however, the first cast added the Snellen eye chart located 50 cm from the video camera to assess visual acuity. The eye chart shows six rows of black letters ranging from 6 mm in the bottom row to 45 mm in the top row (Figure 9). After the night deployment, individual video images for the eye

chart were reviewed by two members. First, using the average of images at each visible depth, and second an instantaneous video image at each visible depth, assigning each row of letters a value of “yes” if the letters could be identified or “no” if they could not. Recorded results were then assessed for visual acuity as a function of estimated lux.

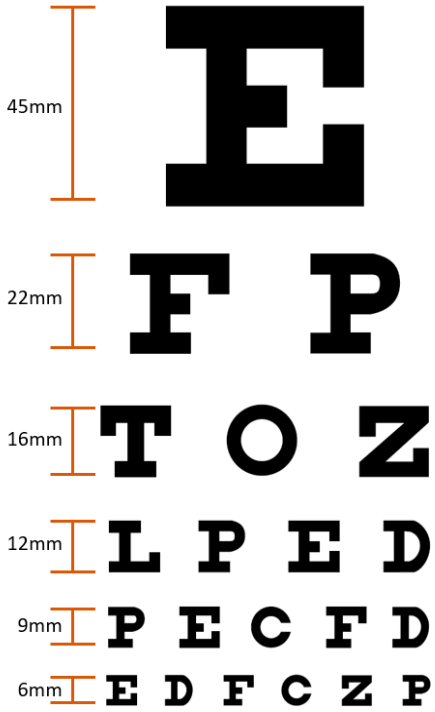

Snellen chart with exact height measurements affixed to Secchi 1 during the third deployment on April 16, 2021 to test for visual acuity.

Figure 9. Adjusted Snellen eye chart.

For this cast, the video camera is fixed at a distance of 0.5 m, resulting in a w=0.72 mm for 0.5 m/0.5 m acuity (Eq.[1]). The lettering on the printed eye chart for the frame is larger (Figure 9). The ratio of the eye chart with sizing relative to 0.72 mm is multiplied by 0.5 m to obtain the distance, as described in the denominator in the acuity ratio. Since this calculation is based on a 0.5 m distance, the numerator (0.5 m) and denominator are multiplied by 12 to describe acuity based on the commonly 6 m/XXX m ratio.

A second cast was performed following the first cast to evaluate object detection with the original three Secchi disk targets at 0.81 m, 1.3 m, and 1.93 m. The pressure sensor

was attached once again to the frame for accurate depth readings, and the RBR Maestro was cast separately for IOPs.

III. RESULTS

A. CAMERA PHONE EVALUATION FOR STATIONARY SETTING AND VARYING EXPOSURE TIME

The camera phone experiment evaluated the exposure time based on longer shutter speeds in a low-light environment for a stationary setting. It is essential to note the camera phone and objects in the camera phone's field of view need to remain fixed to ensure a high level of image sharpness. Any movement by either and the images will become blurry, requiring post-processing outside this project's scope.

The brightness and visibility of camera phone images will increase with decreasing (slower) shutter speeds (Figure 10). Here the candle is the light source, and shutter speeds range from 1/15 s up to 30 s. The garage with standard, overhead, artificial light, shown in Figure 10a, provides the full lux view and contents for reference. The five flags of varying colors and patterns on the back wall served as the baseline in determining the amount of detail seen through varying shutter speed. The overhead lights were turned off, and a single candle is described for the remainder of the images, as seen in Figure 10b-l. Shutter speeds of 1/15 s, 1/10 s, and 1/4 s (Figure 10b-d) show no usable, visible content. 1/2 s shutter speed, (Figure 10e) is the first image that begins to provide a faint outline of the flags on the back wall, and 1 s shutter speed (Figure 10f) shows a clear outline of all five flags. A substantial jump in flag visibility occurs at a 2 s shutter speed (Figure 10g). Words, stripes, and rings can be easily identified, and gym equipment can also be seen in front of the wall. A positive increase in visibility occurs from 4-10 s shutter speeds (Figure 10h-j) until 15-30 s shutter speeds (Figure 10k-l), where the image starts to become oversaturated. The two additional candle locations were performed (not shown) and rendered similar results.

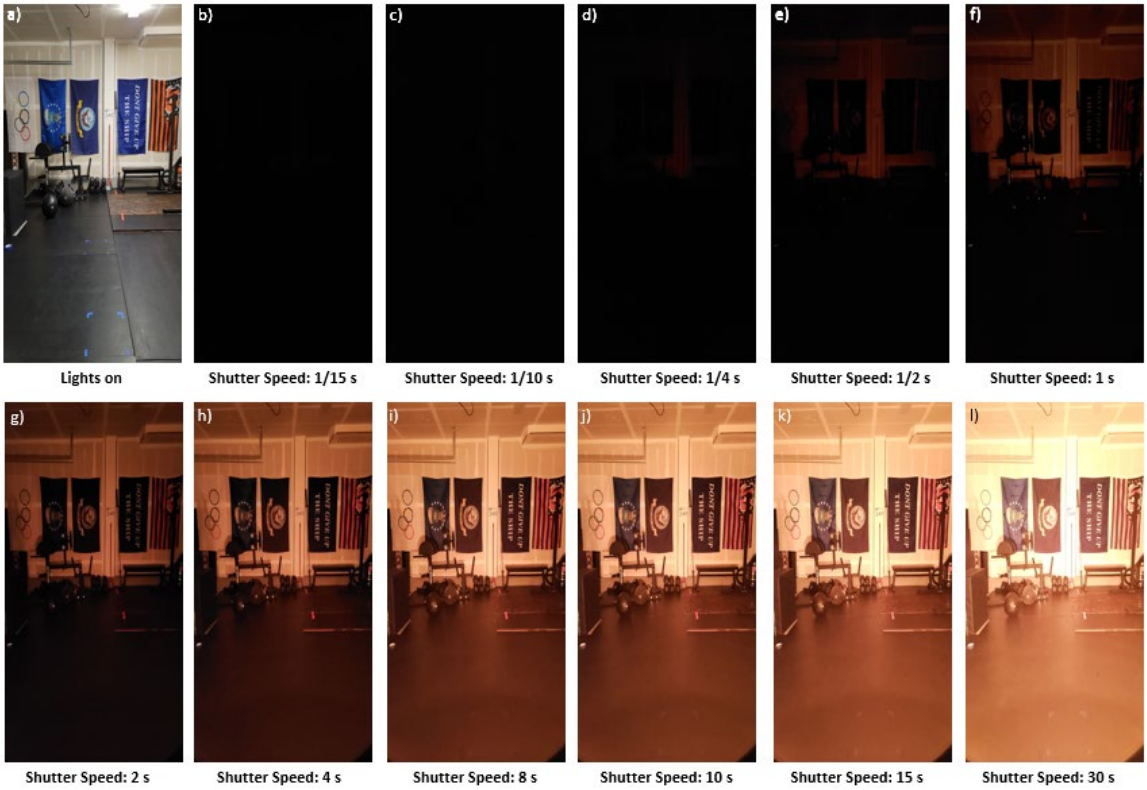

(a) Garage with the overhead light on. (b)-(f) Increasing shutter speed from left to right. The camera remained stationary 5.8 m from the back wall and the candle directly below the camera.

Figure 10. Low-light garage experiment results.

In summary, a stable camera phone with a stable scene and one candle, representing about 1 lux 1 meter away, requires a minimum of 2 s exposure to brighten the nearby scene enough to be visible. This type of stability is not likely for underwater operations. The evaluation with a camera phone with relatively long exposures highlights the difficulty of obtaining a visual scene with an instantaneous (fractions of a second) unstable video camera and a moving scenery in an ultra-low-light environment.

B. UNDERWATER VIDEO CAMERA IMAGES OBTAINED IN A CONTROLLED, LABORATORY TANK

In the following, images for two fixed distances with varying light levels achieved by ND filters are described for the video camera in the laboratory tank. The 36 cm distance between the video camera and two vertically separated square targets is shown in Figure

11. Images are in order of increasing light values (Figure 11a) with a filter resulting in 0.015% light transmission and finishing with a filter resulting in 0.15% light transmission (Figure 11g).

The video camera easily identified object detection of the targets at the lowest light levels and as a step further, the individual letters on the targets can also be identified (Figure 11a-b). Results with the targets facing the camera exceeded expectations however, it is challenging to identify the PVC pole beneath. The PVC pole and targets were turned 180 degrees to evaluate the finer details of the PVC pole and Velcro as seen in Figure 11c-g. When against a light target background, the PVC pole can be identified. As the light intensity increases, additional items such as the filling hose becomes visible in the back left of the tank (Figure 11b-g) and the slotted black boards that line the bottom of the tank (Figure 11g). Changes from one filter to the next did not always render marked differences, for example moving from Figure 11e-f, still it is believed this may be due to the automatic dynamic range of the video camera. The automatic dynamic range is a feature that changes based on the contrast of the setting and changes in available light. There are no controls on this feature for the end-user. This is not believed to be problematic, but it does create slight variations (not shown). No additional testing of the automatic dynamic range occurred since the focus of the laboratory test showed that the video camera could see objects and finer object details in a low-light setting.

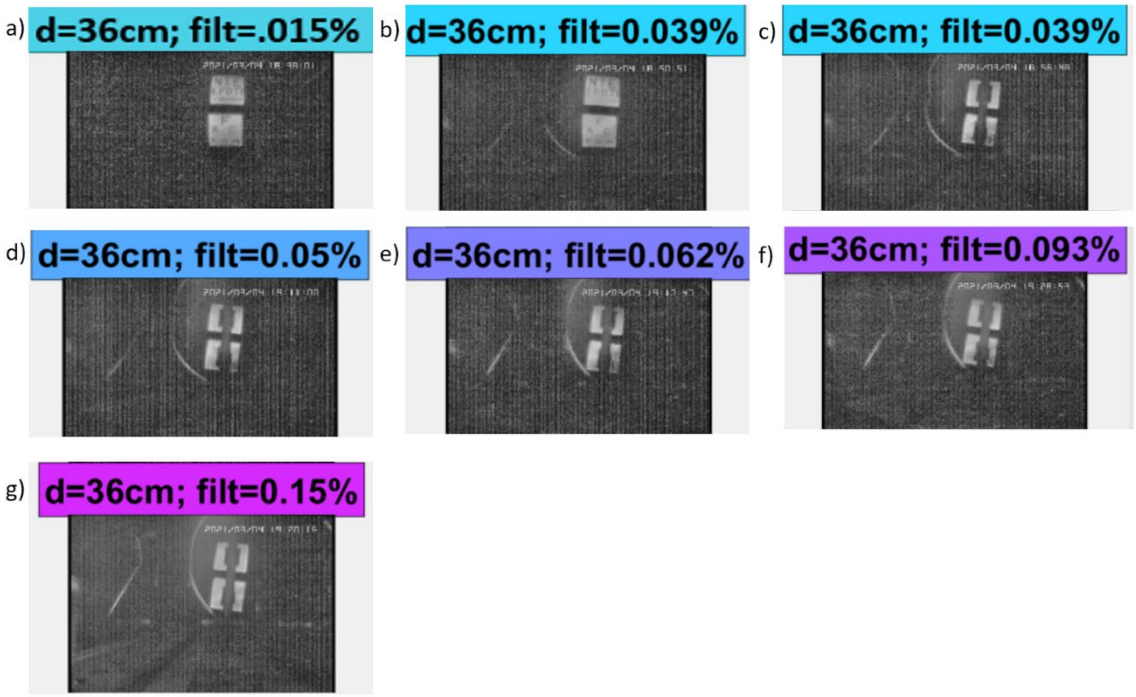

Lab results from the video camera when the targets were 36 cm from the video camera. Figures are in order of increasing light. The percentage refers to the nominal transmission or the portion of light that makes its way through the selected filter(s). (a)-(b) Two white targets stacked on a single PVC pole with letters ranging from 0.63-5 cm facing the video camera (c)-(g) Targets turned 180 degrees to test for fine detail.

Figure 11. Lab results with a target at 36 cm.

Moving the targets back to 66 cm nearly doubled the distance, as was seen in Figure 12. Although some fine detail was lost in recognizing individual letters on the targets (Figure 12a-b), object detection is still validated with ease. The two vertical targets could be seen at every light value. Visibility of the PVC pole and additional objects as light intensity increases continued to hold throughout with the addition of reflected targets off the inside left of the tank. It is recognized in rotating the targets 180 degrees that the experiment evolved into a qualitative evaluation. However, results provided valuable direction for future experimental design. Different distances were also evaluated (not pictured) and had similar results.

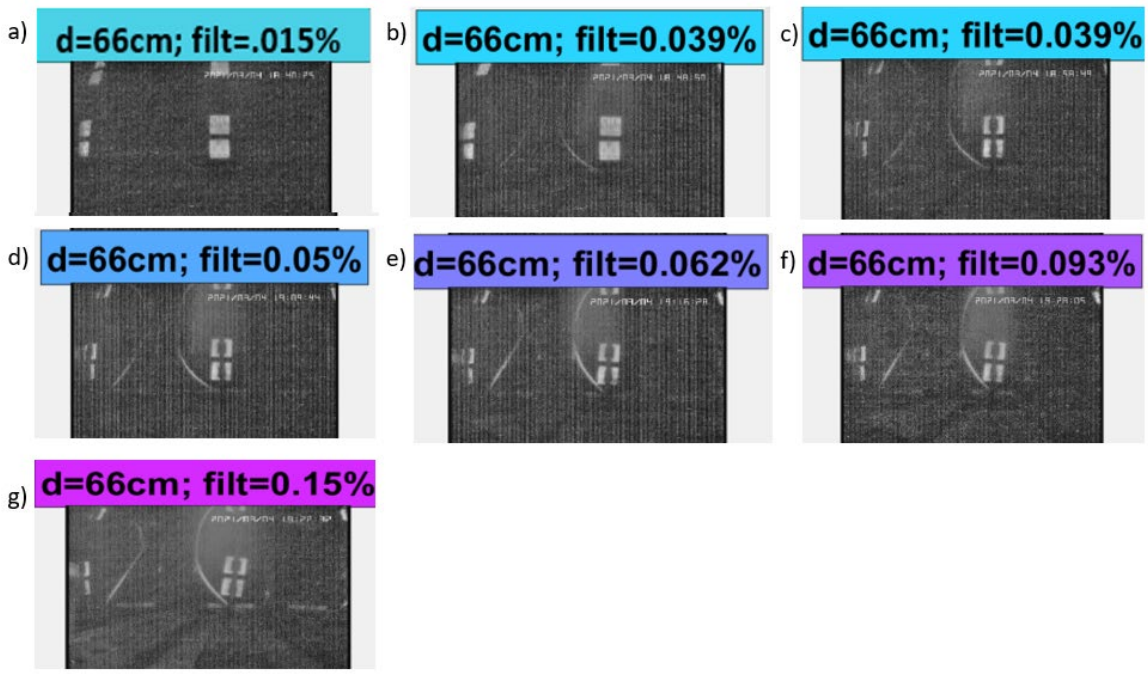

Lab results from the video camera when the targets were 66 cm away. Figures are in order of increasing light. The percentage refers to the nominal transmission or the portion of the light that makes its way through the selected filter(s). (a)-(b) Two white targets stacked on a single PVC pole with letters ranging from 0.63-5 cm facing the video camera. At this distance, the reflection of the targets is seen off the left interior of the tank. (c)-(g) Targets turned 180 degrees to test for fine detail.

Figure 12. Lab results with a target at 66 cm.

C. UNDERWATER VIDEO CAMERA IMAGES OBTAINED IN MONTEREY HARBOR

The vertical casts performed in Monterey Harbor demonstrated both the capability of the frame system to reach depths up to 12 m and the ability of the video camera to capture images throughout the entire water column. With a low surface lux of 0.11, the frame was observed from the surface to the seabed (Figure 13). The video camera worked so well that the detail of the seabed and zip ties were visible. This allowed for a more thorough evaluation of the objects in the video camera's field of view discussed next.

A side-by-side comparison during cast number 3 of the frame system at the surface versus the frame system on the ocean floor was 11.9 m. A reading of 0.11 lux was measured at the surface, and object detection of all three Secchi disks is seen on the ocean floor.

Figure 13. Harbor cast surface vs. bottom.

Image pixelation is a problematic aspect of cameras, particularly those with low resolution and a fisheye lens representing the video camera. This was not an issue in the laboratory tank and the relatively close distances, but pixelation is more of a problem in the field with more considerable distances. The three Secchi disks pixelation differs for the video camera in Figure 14a. Note Secchi 1 is 0.81 m and Secchi 3 is 2 m from the video camera. The pixelation of Secchi 3 reduces the ability to detect edges that are further influenced by low-light noise when deployed at deeper depths with less light. The recognition of edges is provided in Figure 14b-c. Edge detection at the surface for cast 3 of the three Secchi disks is shown in Figure 14b. Secchi 1 supports the highest level of edge detection at the intersection where the Secchi disk changes from black to white and at the two bolts on the front of the disk. Secchi 2 shows a fair amount of detail. However, there is a definite decrease in sharpness, especially around its outer edges, compared to Secchi 1. The center point of the Secchi 2 is also far less defined. Finally, Secchi 3 shows

the slightest amount of positive edge detection, particularly where the black outer edge meets the dark background. Secchi 3 is also the only disk that did not have its bolts identified due to pixelation.

The detection of fine details, such as the bolts in Secchi 1-2, observed in the Monterey harbor casts transition in evaluating the video camera from object detection to object visibility. Mean edge detection over the entire cast is shown in Figure 14c. The red color represents an edge that has been detected throughout the whole frame cast, and the solid blue color represents regions where there were never any edges detected. Transitional colors represent partial detection, where warmer colors indicate a higher percentage of occurrence (Secchi 1), and cooler colors represent a lower occurrence (Secchi 3). Nearly all of Secchi 1 edges were detected throughout the cast, as indicated by the heavy presence of red to include the outer edges, interior intersections, and two bolts on the bottom. Secchi 2 did show some positive results within the interior intersections. However, colors were much cooler around its outer edges. Finally, Secchi 3 showed the most variability in mean edge detection, with only the vertical line of intersection down the center having consistent edge detection.

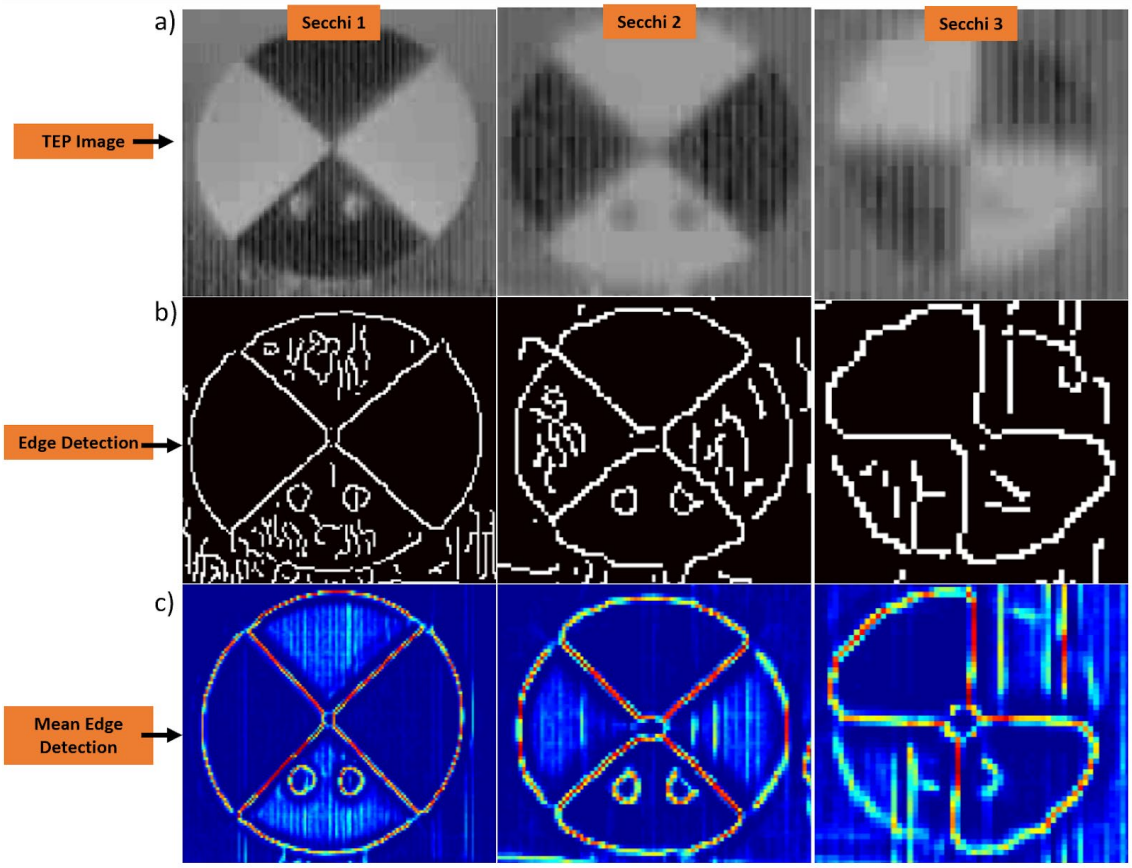

(a) Zoomed views of the three Secchi disk targets captured by the video camera. A drastic change in the pixel size can be seen moving from the closest disk, Secchi 1, to the farthest disk, Secchi 3. (b) Resultant images after using edge detection within MATLAB. (c) Mean edge detection of the three targets. Red indicates areas where edges were often or always detected, and blue indicates areas where no edges were detected.

Figure 14. Edge detection of three Secchi disk targets.

Vertical stacks of Secchi disk edges are plotted with a slight offset as a function of depth in Figure 15 to evaluate variability in edge detection of the five harbor downcasts. All five casts are provided in one Figure for completeness. A representative edge results in a near circular line with a cross in the center (Figure 15). Discontinuities in the circle highlight when the edge detection failed. For example, in the 6-7 m range on cast 2, the 3-4 m range on cast 4, or a majority of cast 5, the Secchi edge detection partially failed. It is hypothesized this is either due to material in the water column impeding the video camera's view or when the video camera's dynamic range over-adjusted the background water column relative to the white portion of the Secchi disk. In general, edge detection

recognized Secchi 1 throughout most casts, even in the darkest and deepest part of the harbor casts. The video camera had no issue maintaining object detection of Secchi 1 from the surface to the ocean floor.

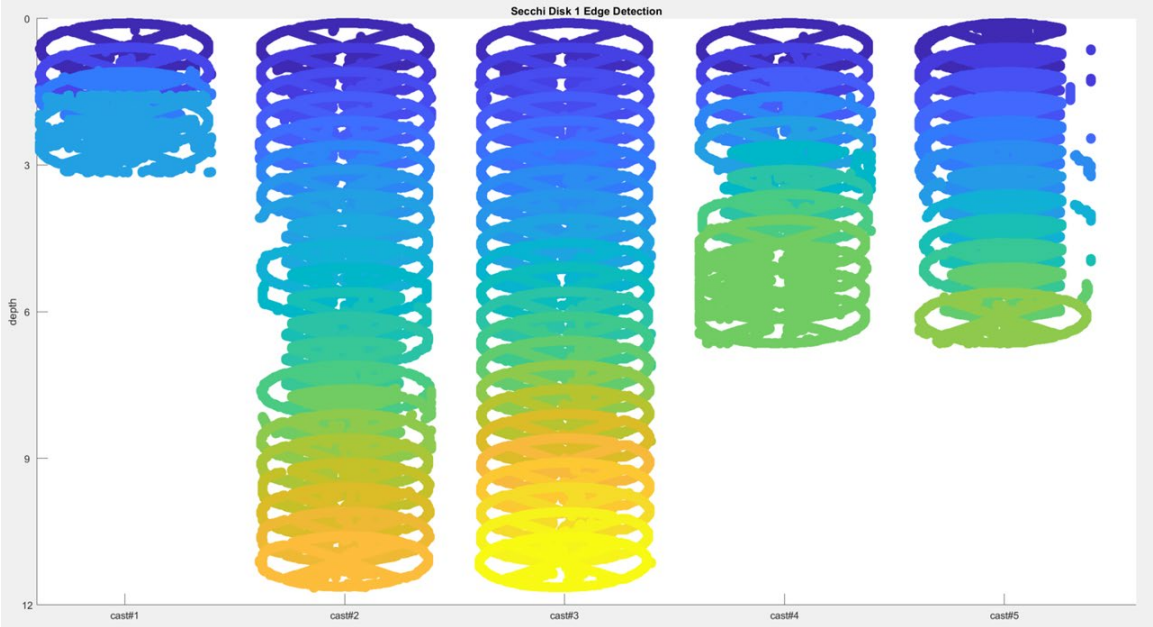

Edge detection of Secchi 1. Casts 1-4 took place at the Breakwater Cove Marina at depths ranging from approximately 3m to just under 12 m, and cast 5 took place at Municipal Wharf 2 at a depth of 6 m. The color change from blue to yellow reflects the change in depth.

Figure 15. Edge detection of Secchi 1 from surface to bottom.

Similar edge detection was performed for all five harbor casts for Secchi 3 as a function of depth (Figure 16). As discussed earlier, Secchi 3 had the most pixelation causing the circle's edge to have significant discontinuities, even at the surface. As expected, the circular discontinuities increase with increasing depth. The interior crosses present within the Secchi disk are also distorted with increasing depth. Secchi 3, in an object detection sense, is visually there, but the fine details are lost both as a function of pixelation and camera noise with lower light levels. The object is observed throughout the entire water column, so this is a positive result. The 2 m horizontal distance is nearing a limit for which the fine details of an object can be recognized.

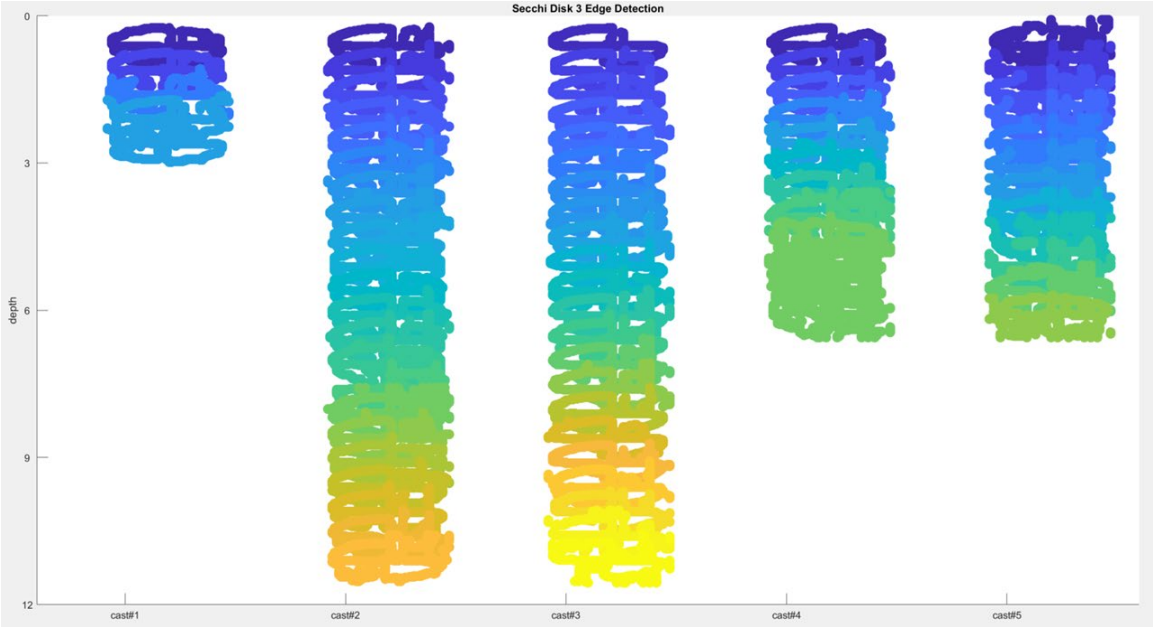

Edge detection of Secchi 3. Casts 1-4 took place at the Breakwater Cove Marina at depths ranging from approximately 3 m to just under 12 m, and cast 5 took place at Municipal Wharf 2 at a depth of 6 m. The color change reflects the change in depth.

Figure 16. Edge detection of Secchi 3 from surface to bottom.

Bulk IOP results across all five casts remained reasonably consistent (not shown). Cast 3 results were selected because it had the most extensive sample depth, 12 m, for CDOM, chl_a, and Turbidity (Figure 17). CDOM levels ranged from 0.8-1.2 ppb, chl_a are close to 0 μg/L, and finally, most turbidity ranges from approximately 0.4-1 NTU; however occasional peaks were observed out to 1.5 NTU. It will be essential to have these relative baseline IOPs for reference compared to open ocean deployments (discussed next).

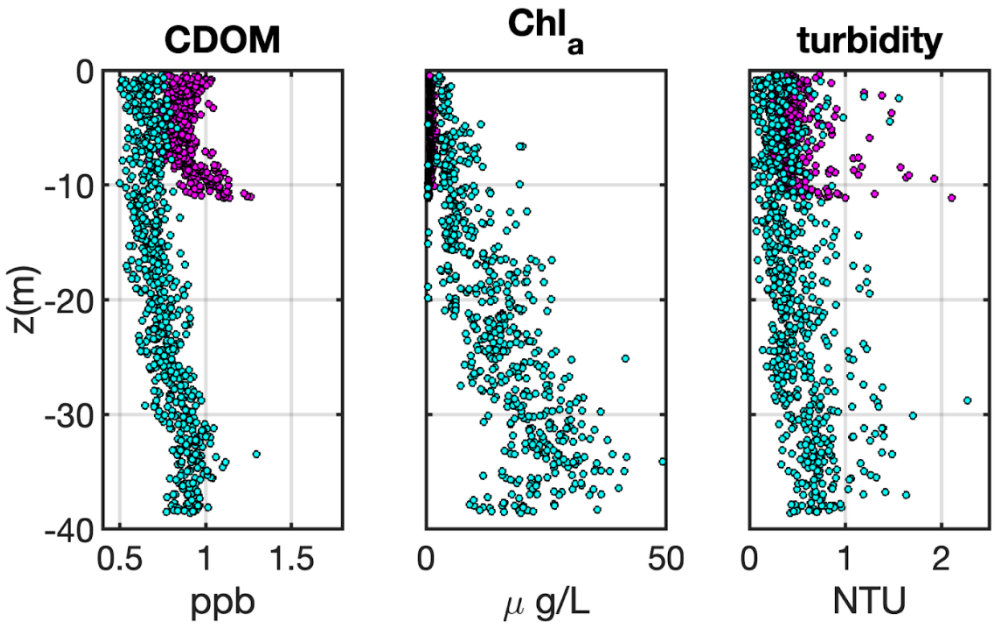

RBR Maestro IOP cast 3 (magenta) from Breakwater Cove Marina on March 24. CDOM, chl_a, and Turbidity are measured from the surface down to a depth of ~12 m compared to the open ocean cast (turquoise) from April 13. CDOM, chl_a, and turbidity are measured from the surface down to a depth of ~40 m.

Figure 17. March 24 IOP cast from Breakwater Cove Marina.

D. UNDERWATER VIDEO CAMERA IMAGES OBTAINED IN THE OPEN OCEAN

The first open ocean deployment was the first field test of the video camera in a low-light underwater setting. The deployment occurred shortly after sunset to evaluate the varying lux associated with the sun's position due to the video camera's uncertainty. Close attention was paid to the decreasing light levels of sunset, civil twilight, nautical twilight, and astronomical twilight (Figure 18a). All casts took place after sunset, 1657, and before astronomical twilight at 1827 (Figure 18b). A total of 5 casts were evaluated and within a 20 min time span, results jumped from full object detection of targets, ~20 m in casts 1 and 2, to almost no object detection, casts 3,4 and 5 (Figure 18c). Casts 1 and 2 did have a higher light availability since they occurred closer to sunset. However, the extreme drop off in object detection of cast 3 was completely unexpected based on video camera specifications and remaining light availability. Ultimately, these results suggested that the video camera was underperforming, and the video camera was returned for re-

configuration. The test was not an entire wash, as it did validate our framing system for ocean testing. The fundamental question remained could the video camera see in a low-light underwater setting.

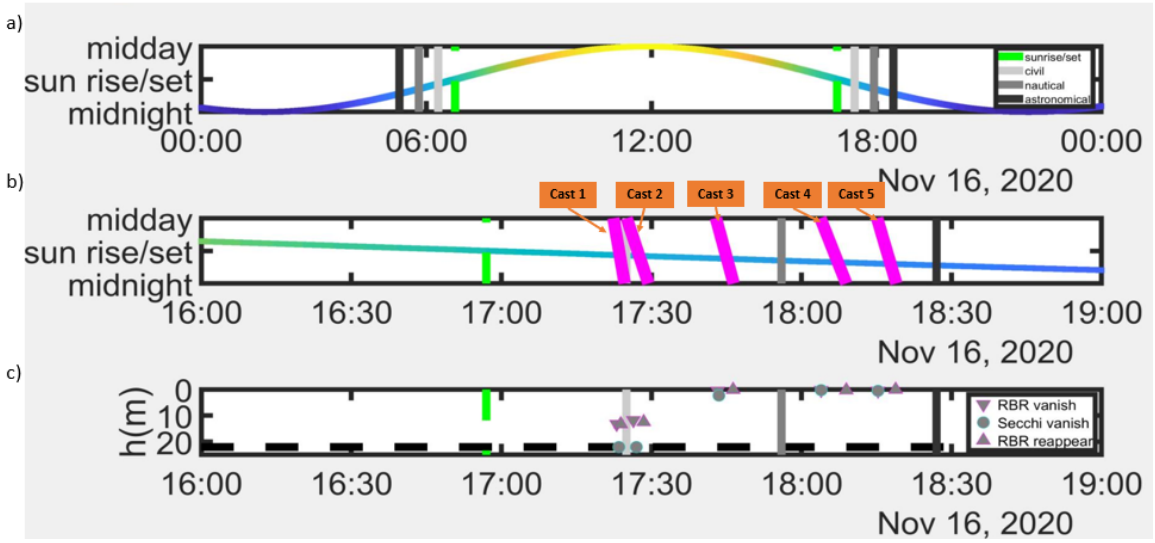

(a) Available sunlight within a 24-hours. Black lines indicate astronomical sunrise/sunset, charcoal lines indicate nautical sunrise/sunset, grey lines indicate civil sunrise/sunset, and finally, green lines indicate sunrise/sunset. The overarching line indicates the sun's position in the sky relative to the time on the x-axis. (b) Time has been focused to 16:00-19:00 and the pink diagonal lines are the 5 casts performed in the open ocean on November 16. (c) Grey outlined shapes indicate the Secchi disks and RBR solo sensor with the video camera per each cast. Outlined pink triangles facing downward indicate when the RBR solo disappears in its downcast and upward pink triangles when it reappears in the upcast returning to the surface. Turquoise outlined circles similarly indicate Secchi disks. The dashed line at the bottom indicates the maximum depth of casts.

Figure 18. November 16 open ocean casts as related to available sunlight.

Before discussing the second deployment, it is essential to examine the larger chl_a observed in the open ocean on March 29 (not pictured) and again on April 16 as compared to the results that were seen less than a month prior during the harbor casts (Figure 17). Due to an algae bloom within the open ocean of Monterey, chl_a from the IOP measurements showed a significant increase compared to the near 0 within the harbor. Past 5 m, chl_a increased steadily with depth from about 10-40 µg/L at 40 m. Since chl_a is a dominant light-harvesting pigment and is universally present in cyanobacteria or "blue-

green algae," these measurements help to confirm the extensive amounts of bioluminescence that were observed by the video camera on both March 29, and April 16.

The second ocean deployment on March 29 provided additional lessons learned. Still, it was difficult to find substantial amounts of usable data amidst the violent jolts of the frame system forced by rough seas (Figure 19a). Additionally, heavy bioluminescence obstructed the view of the targets almost completely beyond 12 m (Figure 19b). Edge detection was unavailable due to the concentration of bioluminescence, however when the video was analyzed frame by frame, there were glimpses of Secchi 1 that can be seen as deep as 23 m (Figure 19b). The bioluminescence video fouling was overlooked as the culprit until the last deployment.

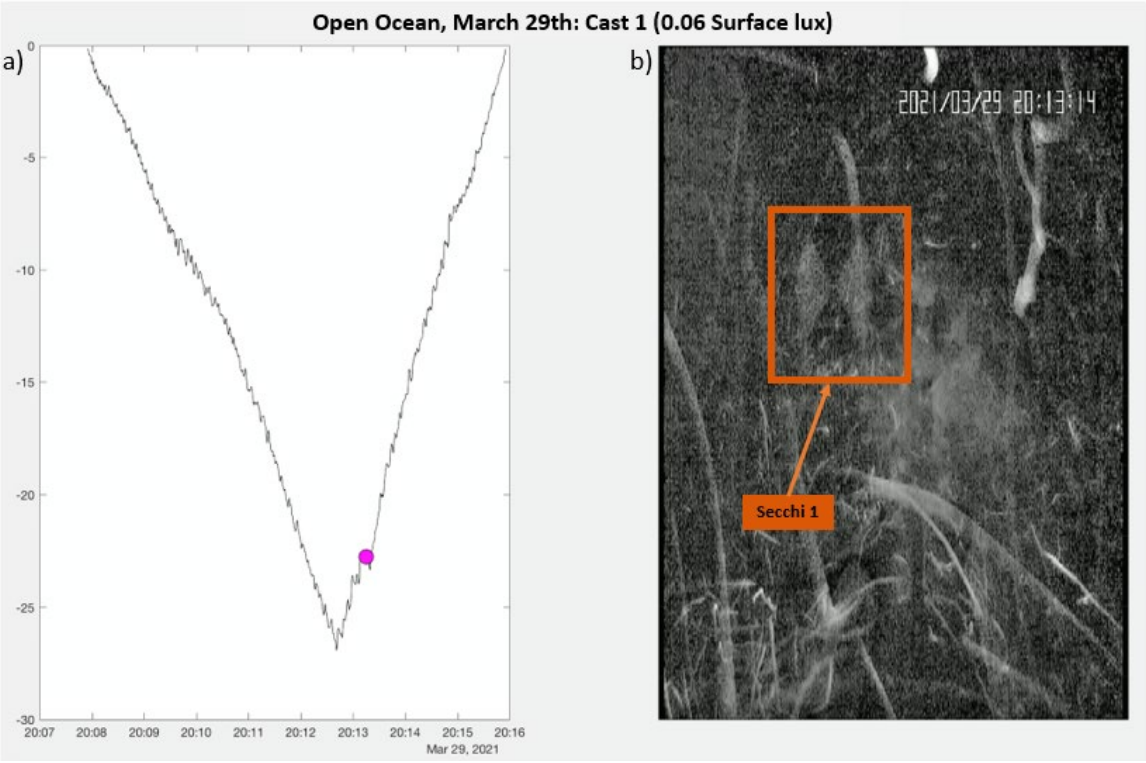

(a) Depth of the frame vs. time as it was lowered to ~26 m on March 29. The jolts of the frame due to seas can be seen by the jaggedness of the depth line as the frame was lowered and raised. (b) Object detection of Secchi 1 surrounded by bioluminescence at ~23 m.

Figure 19. March 29 open ocean object detection results at 23 m.

The final ocean deployment on April 16 built upon lessons learned and incorporated a new element, the Snellen eye chart, to test for visual acuity. This deployment showed promise from the start with substantially calmer winds and seas noted by the vertical smoothness in the depth measurements (Figure 20a). Additionally, pauses in the upcast are seen as steps every 5 m. This was done to allow the video camera time to auto-adjust to the new light levels. A surface measurement of 0.02 lux was recorded for both casts. From the video images measured on the March 29 deployment, object detection of Secchi 1 was expected to fall at 25m. This was validated through a similar frame-by-frame analysis as the previous deployment and shown in Figure 20b. Edge detection was once again unusable on the Secchi disk cast because the heavy concentration of bioluminescence throughout the deployment contaminated the video images.

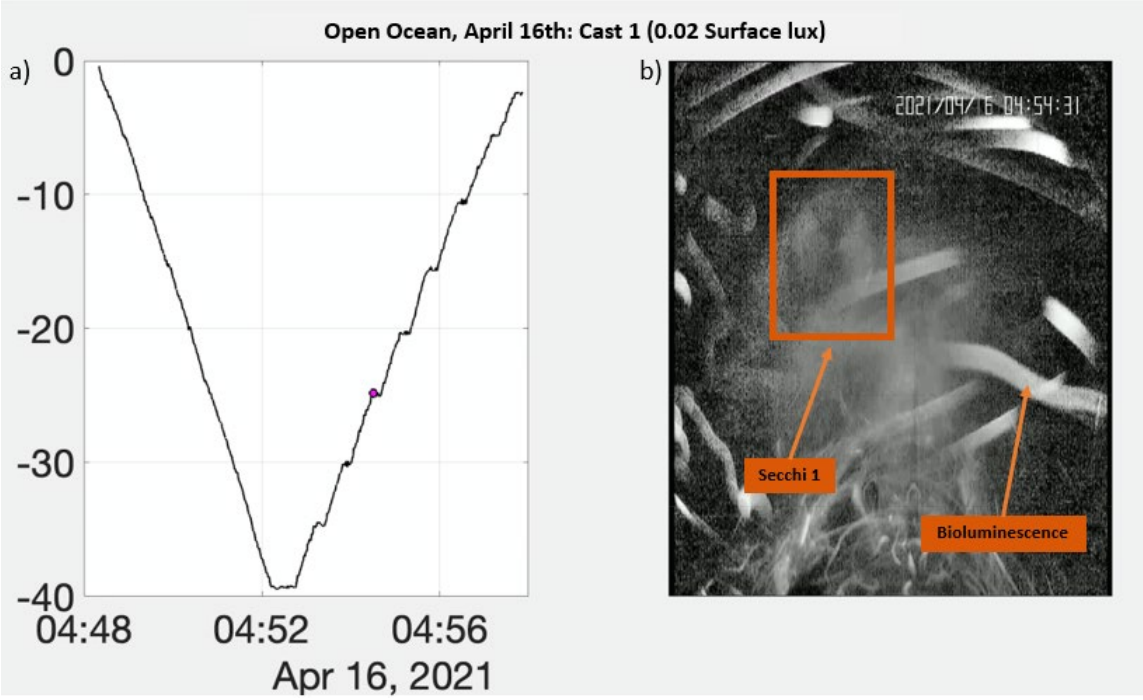

(a) Depth of the frame vs. time as it was lowered to ~40m on April 26. The frame has a smooth cast as it was lowered to 40m, and 10s pauses for video camera focusing can be seen every 5m on the upcast. (b) Object detection of Secchi 1 surrounded by bioluminescence at ~25 m.

Figure 20. April 16 open ocean object detection results at 25 m

The additional cast of the Snellen eye chart, 50 cm from the video camera, provided other fine object detection and provided a quantitative measure of visual acuity as the frame was lowered to 40 m. As mentioned earlier, results were not entirely clear due to heavy bioluminescence. Still, an average of the images captured at each depth allowed for a general idea of how object detection and visual acuity decrease with depth (Figure 21). Of note, images were individually analyzed for visual acuity on a larger scale; resized to provide a side-by-side comparison. A silhouette of the target could easily be identified to approximately 25 m, and it could be argued that a faint silhouette is still present up to 31 m.

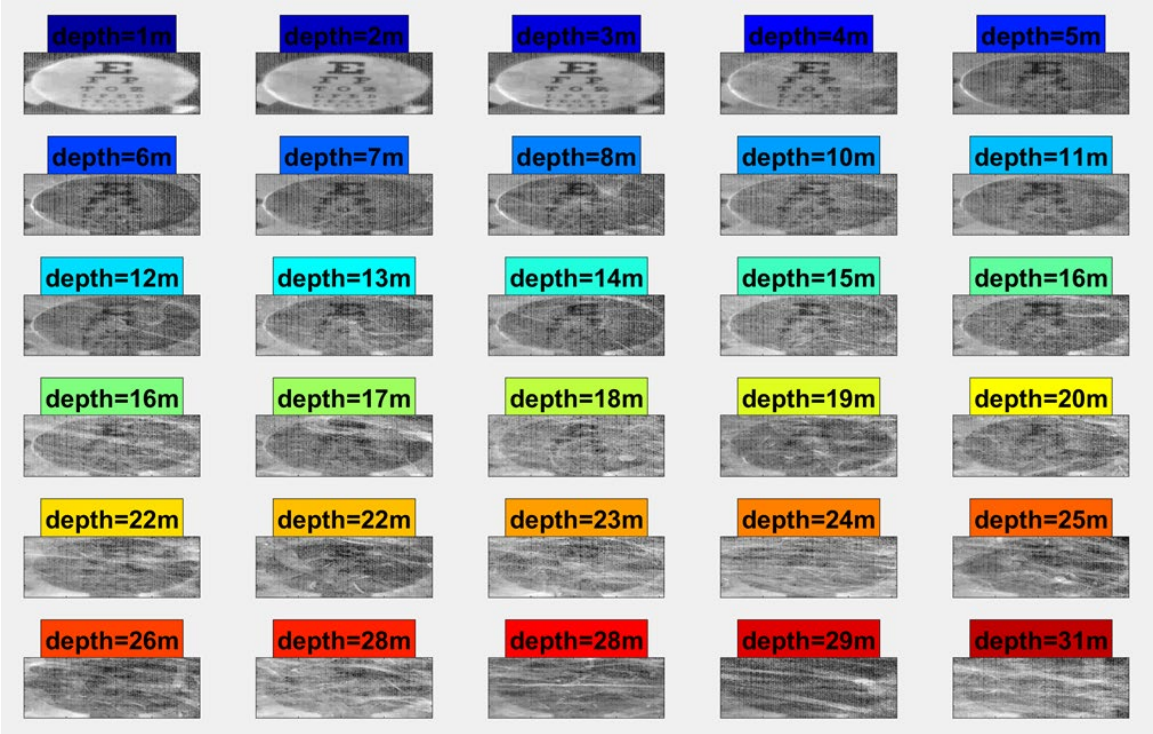

Object detection of the video camera using the Snellen eye chart ~50 cm away. Images were captured as the video camera frame system was lowered into the open ocean. Most images increase 1m in depth up to 31 m. There are some duplicate depths, however, the images are different.

Figure 21. April 16 open ocean Snellen chart.

A broad analysis of visual acuity identified a sharp decrease after the 4 m depth (Figure 21), where the bottom two rows of letters could no longer be seen. And once again,

beyond 12 m, the top row, large E, remained the only letter visible on the chart. It is difficult to identify any letters past 16m in this representation. A more comprehensive analysis of the Snellen chart cast resulted as one might assume in that both the average and instantaneous images, multiple rows received "yes" values close to the surface (Figure R22a). As the frame moved further from the surface, fewer and fewer rows could be identified (Figure R22b).

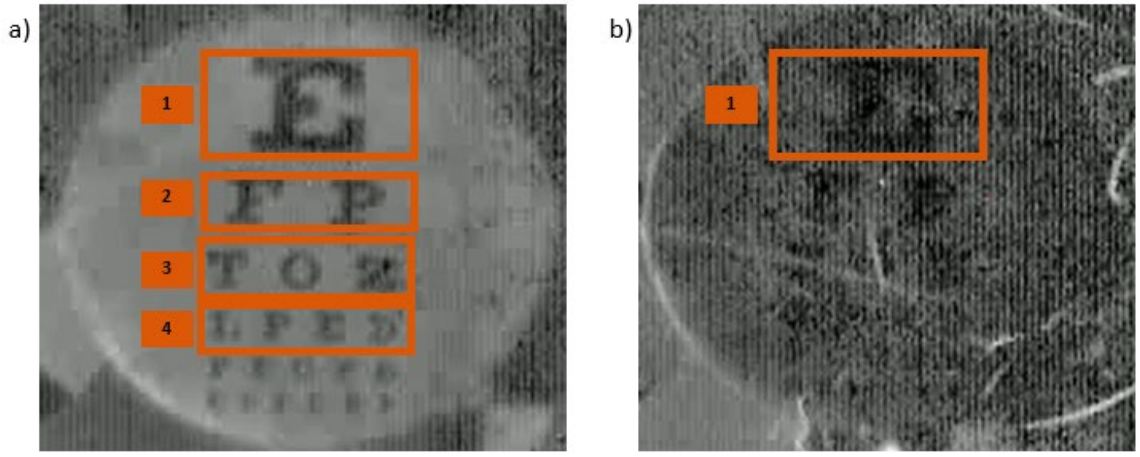

Snellen eye test to evaluate visual acuity. If the letters in the row could be identified, the row was assigned a value of "yes" (a) An example of positively identified rows 1-4. (b) An example of the eye chart at a deeper depth where rows were more challenging to identify.

Figure 22. Open ocean Snellen acuity chart.

Results from the average and instantaneous images as described above were plotted below, comparing their Snellen acuity vs. the estimated lux values (Figure 23). At the surface, the highest lux levels experienced the highest acuity (smallest number). Contours were identified as small as those in the fourth row, with 12 mm spacing. For this, it was assigned an acuity value of 6 m/99 m, where 6 m is the adjusted distance between the camera and the target and 99 m is the distance at which a person with 6 m/6 m, perfect vision, could identify the same row of letters. Both the instantaneous and average images received the 6 m/99 m acuity as it was lowered into the first few meters of the ocean. The acuity of the instantaneous images quickly declined as lux levels approached 0.005 lux with a brief acuity of 6 m/132 m, 6 m/182 m, and finally a majority of 6 m/371 m where

only the large “E” could be identified. The average images held a higher acuity of 6 m/132 m for a few meters and then 6 m/182 m to ~0.00025 lux. At an approximate depth of 15 m, both average and instantaneous images lose all acuity. It is difficult to account for the effect of bioluminescence in the acuity testing. The low-light sensitivity video camera undoubtedly prevented the auto-iris control and dynamic range from functioning correctly and affected our ability to identify additional rows.

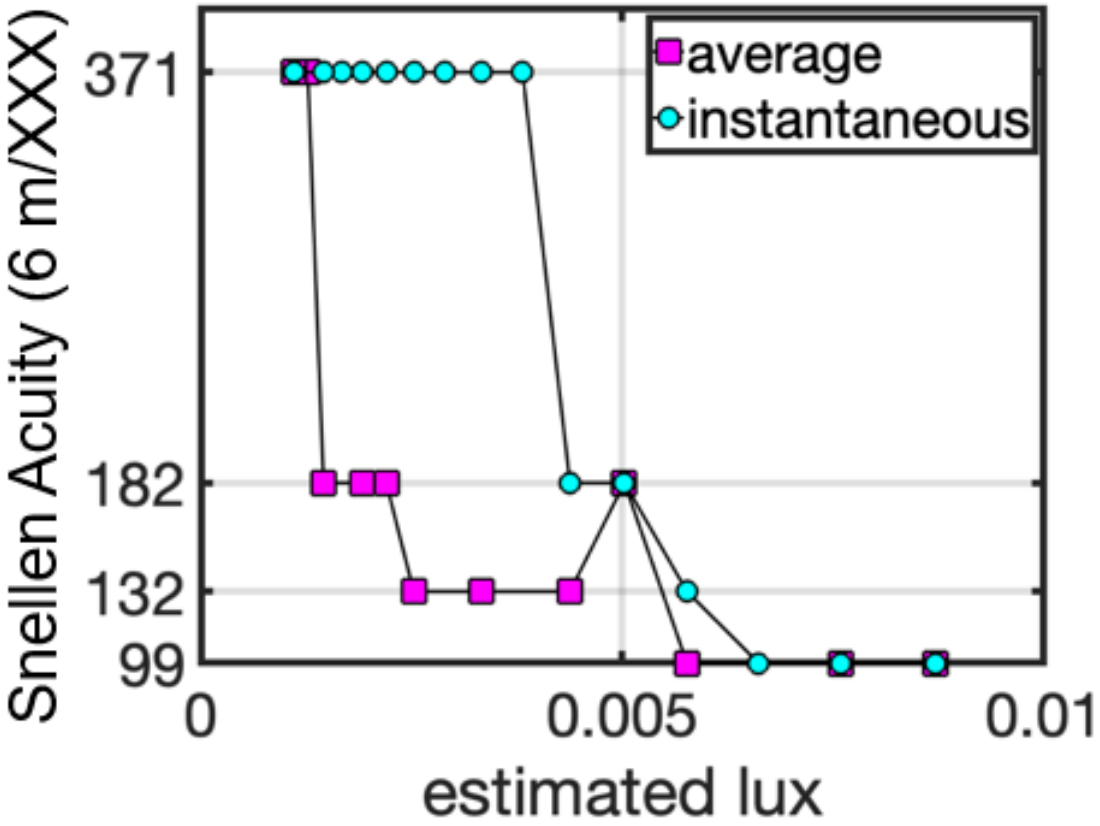

Visual acuity of the video camera with a Snellen eye chart ~50 cm away. The magenta shows the average visual acuity of the video camera as the frame was lowered into the water (decreasing lux). The turquoise shows the instantaneous acuity of the video camera at each respective depth as the frame was lowered. Lux levels on the x-axis were calculated as a function of depth.

Figure 23. Average vs. instantaneous visual acuity with decreasing lux.

THIS PAGE INTENTIONALLY LEFT BLANK

IV. DISCUSSION

A. COMPARISON WITH NVGS

NVGs are commonly known to enhance the human ability to see and successfully operate in low-light conditions on land (Parush et al. 2011). Underwater low-light cameras, on the contrary, are not very commonly known or studied. The following section will discuss some of the major findings in the evaluation of the video camera as compared to the readily available information and research provided for NVGs.

A direct comparison of Snellen acuities of the video camera at average and instantaneous acuity was made to Gen III NVGs (AN/AVS-9 F4949) (Figure 24). The NVG visual acuity was based on the Landolt C method. According to Pinkus and Task (1998), participants needed to identify the letter C and detect the correct orientation of the gap in the C with the NVGs ~9.14 m away at varying light levels. Afterward, the Landolt C results were transformed to Snellen acuity (Pinkus and Task 1998). The NVGs significantly outperformed both the average and instantaneous video camera acuities, remaining near-perfect. However, the underwater acuity tests were influenced by bioluminescence. Acuity suggests that the visibility underwater will be limited to much closer ranges than NVGs on land.

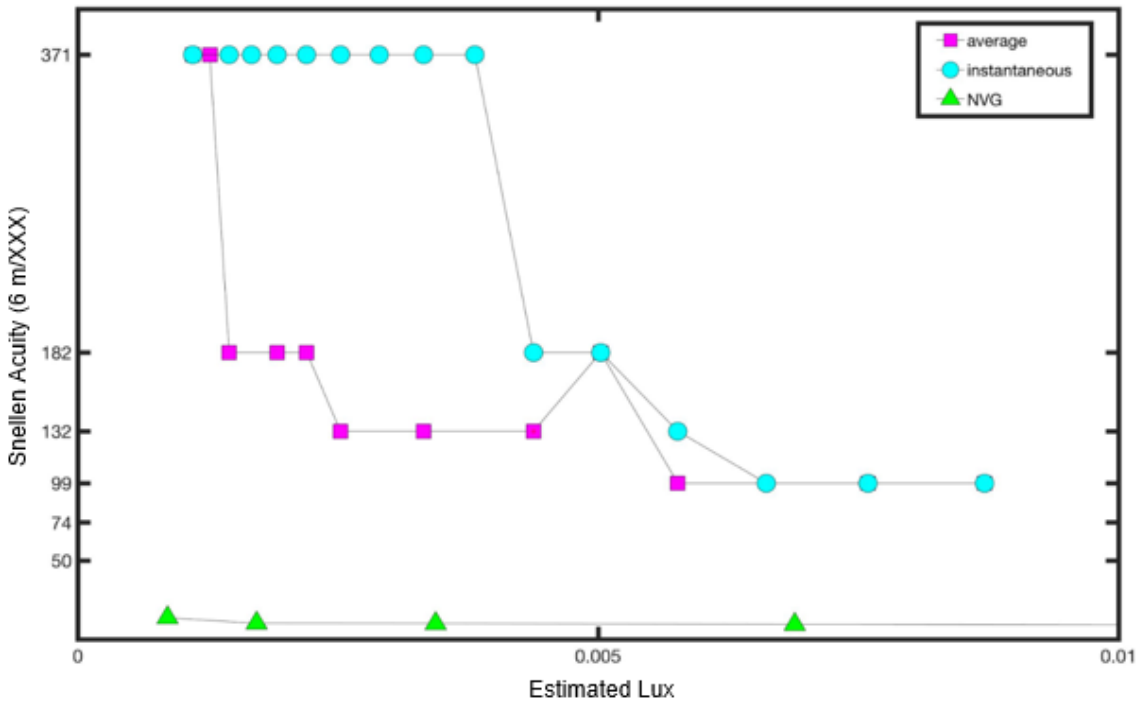

Visual acuity of the video camera with a Snellen eye chart ~50 cm away. The magenta shows the average visual acuity of the video camera as the frame was lowered into the water (decreasing lux). The turquoise shows the instantaneous acuity of the video camera at each respective depth as the frame was lowered. The green triangles show the 95% probability visual acuity of NVGs. Lux levels on the x-axis were calculated as a function of depth.

Figure 24. Visual acuity of the video camera vs. NVGs.

The Snellen letter chart provided an initial assessment of visual acuity for the video camera. Still, additional tests can provide a more precise evaluation that eliminates human inconsistencies. According to Pinkus and Task (1998), in NVGs, limiting resolution is the spatial frequency at which the modulation transfer function (MTF) of the NVGs and the visual threshold function (VTF) intersect. The intersection occurs at the highest spatial frequency. The NVG provides enough contrast for the human eye. The MTF estimates can be converted to a Snellen acuity for comparison with other testing methods (Pinkus and Task 1998). Before the current technology, acuity testing involved several humans and many tests to recognize patterns, such as USAF 1951 tri-bar resolution chart. An individual's judgment often led to inconsistencies. Today, through ISO charts, a similar process can be performed and analyzed using software to pinpoint a more exact acuity.

In thinking about the real-time advantage of NVGs, attempting to create an underwater equivalent is no easy task. This video camera would not operate concurrently with an underwater monitor because it would generate too much ambient light. On the other hand, if the ability to use the low-light technology found within the video camera, or if the ability to create a feed of some sort into real-time underwater goggles were an option, this could be a capability worth exploring.

B. OBJECT DETECTION AND VISUAL ACUITY IN AN OPERATIONAL SENSE

Although object detection should be a fairly straightforward test of whether an object can be seen, trying to quantify exactly how well it could be seen turned into a bit of a grey area. Beyond the edge detection analysis performed in post-mission processing (Figure 14-16), when someone is in the operational environment, real time detection is not necessarily as clear cut. It becomes more of a question of if something can be seen well enough to influence important decisions. This is largely the reason for taking a step beyond object detection into the testing of visual acuity (Figure 22-23).

Unfortunately, attempting to define visual acuity in the underwater low-light environment proved to be equally as difficult to quantify as there was little to no information available to provide much context into what we attempted to determine. The video camera indeed demonstrated its baseline effectiveness in terms of object detection (Figure 15). Still, because of the pixel size, noise, and decreased resolution moving into increasingly lower lux levels, the sharpness of images was lost that otherwise might have been identified (Figure 16). In reality, some of the details we tried to quantify to give the video camera a measure may not have been fair considering the likely operations it would be designed for. For example, it is pretty safe to say that most nighttime underwater operations will not require the visual acuity necessary to read anything underwater (Figure 22). Still, it could be argued that performing the Snellen cast provided a baseline for the future to determine the size or outline of objects one can expect to see at a certain depth, lux level, or distance (Figure 23).

As an additional point, these metrics remove our natural bias. During operations, the human tendency will provide additional information that has been intentionally discarded within the tests herein, allowing an operator further into lower light environments based on experience—identifying an expected object versus an unknown object. Due to our human bias, it is fair to say that this video camera could see extended results, but this is only if factors like the auto-iris and dynamic range do not become oversaturated in-situ.

C. PERFORMANCE OF THE AUTO-IRIS AND DYNAMIC RANGE

Aside from its fisheye lens, to be successful in low-light underwater environments, this video camera is dependent on the performance of the auto-iris and dynamic range. Ideally, these two attributes allow this video camera the enhanced ability to auto-adjust to any environment or scenario it may encounter. Still, like all technology, it does have its limitations. One such restriction occurs when there are sudden, dramatic adjustments in the lighting. An example of this is the video camera's reaction to turning off the lights (Figure 25). Although the video camera automatically responded and produced a reasonable image in ~6 sec (Figure 251b-i), certain operations do not have 6 seconds to give and require a more seamless transition. In reality, jumping from full to complete darkness may not be a fair evaluation of a video camera designed for low-light environments. Still, it is not out of the question to keep this extreme case of auto adjustment in mind in the event of an unexpected bright flash, where the video camera would respond similarly.

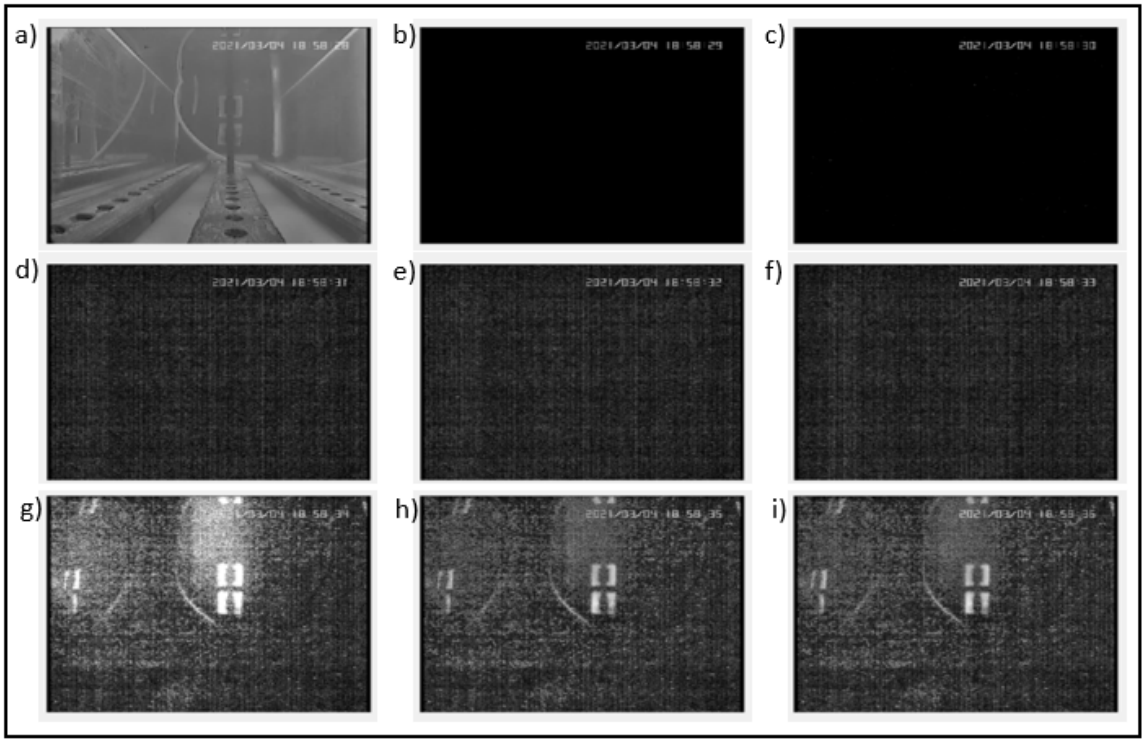

Frame by frame 9 s time series of the video camera's auto-iris and dynamic range adjustment. (a) Video camera in the lab tank with two white vertically stacked targets downrange. Overhead lights are on in the lab. (b)-(i) Same tank configuration with all lights turned off.

Figure 25. Video camera's auto-iris and dynamic range adjustment.

It is also essential to consider if we have an overly bright object in the field of view (Figure 26). In this scenario, the auto-iris will be operating at its minimum aperture, allowing the least amount of light in, and the dynamic range will reach its upper limit, or the video camera's ability to adjust contrast to a usable level. Once the dynamic range is exceeded, all the user will see is the bright white originating from that object. Depending on how far the range is exceeded, the object can be thoroughly washed out, and its surroundings become filled in with noise. Oversaturation can be a major problem if you think you identify one object when there could be additional danger hiding in the background. It becomes crucial to recall what was mentioned above regarding human biasing. Suppose an operator is well trained and has baseline knowledge of what sort of environment they will be operating in and what extenuating circumstances they may encounter. In that case, an operator should use biasing to their advantage to focus the video

camera away from direct light sources and find surrounding silhouettes and patterns. This approach could potentially allow operators to go into even dimmer light than assessed up to this point.

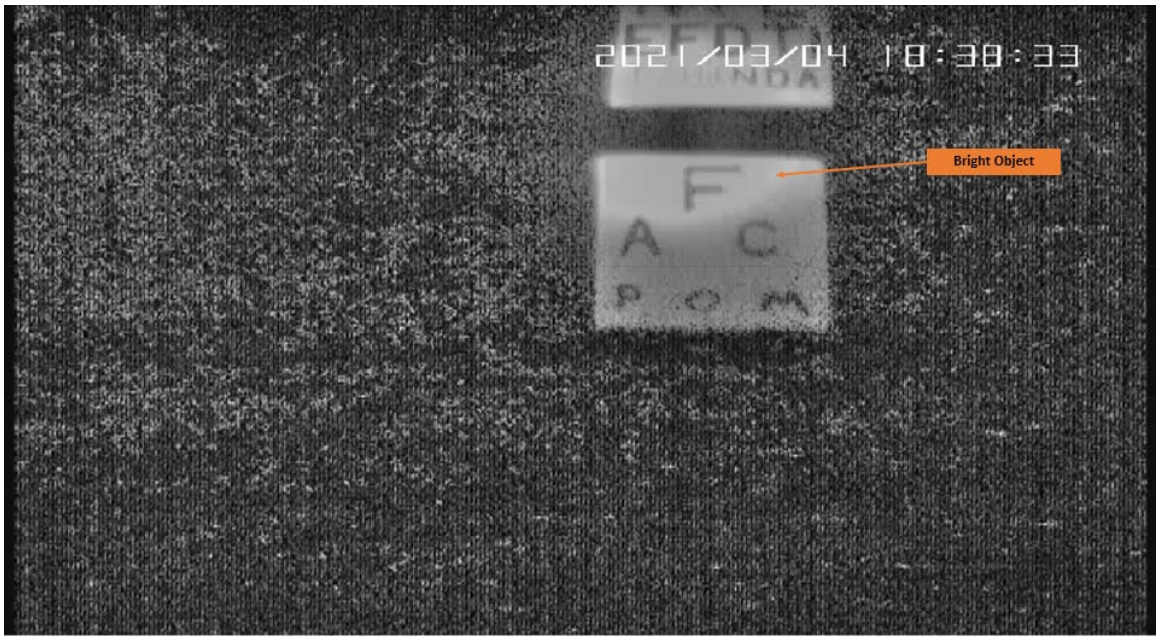

The noise produced by the video camera's dynamic range surrounding an overly bright target.

Figure 26. The noise surrounding the dynamic range of video camera.

D. IS BIOLUMINESCENCE HARMFUL OR HELPFUL IN LOW-LIGHT SCENARIOS?

Here are a few points regarding the bioluminescence encountered during the final two open ocean deployments. Although bioluminescence turned out to be problematic for our basic testing, it may not be difficult if the video camera is co-located with the user and not on a frame. Theoretically, most of the bioluminescence stirred up will end up behind the user, leaving a clear pathway for the video camera as the user moves forward through the water. On the other hand, bioluminescence may be something to take advantage of regarding object detection as it could provide a faint, temporary light source for the video camera. Bioluminescence may not necessarily offer precise object detection. However, it could give brief glimpses of possible outlines of objects seen in open ocean deployment 3,

where the frame stirred up enough bioluminescence to identify silhouettes of targets at upwards of 25 m.

THIS PAGE INTENTIONALLY LEFT BLANK

V. SUMMARY AND CONCLUSIONS

A low-light underwater video camera was tested to evaluate its performance at nighttime with near-zero surface lux to identify an approximate operational depth. The Teledyne Bowtech Explorer Pro low-light underwater video camera was selected for its unmatched low-light sensitivity and underwater-focused design. Minimizing all in-situ light was a top priority, so a data logger was integrated with the video camera and placed within an underwater housing for post-deployment analysis. The video camera and set-up were evaluated through a series of laboratory tests at Naval Postgraduate School and harbor and open ocean deployments in Monterey Bay, CA. The video camera and electronics housing were outfitted onto a 2 m aluminum frame with multiple targets designed at varying distances along with the frame for ocean deployments. The frame was designed as a lightweight that a single person could deploy. Validation of object detection was pursued herein.

The video camera worked well and proved as a capable resource for underwater low-light operations. Black-and-white Secchi disks were observed at 0.50-1.93 m distances. Harbor testing provided object detection to 12 m depth with surface lux <0.2 lux, and open ocean testing indicated object detection to 25 m depth with a surface lux of only 0.02 lux. Due to these promising results, research goals shifted from basic object detection to visibility.

Underwater visibility in the video images was evaluated through visual acuity, defined as the ability to detect letters of various sizes using a modified Snellen eye chart at a fixed distance of 50 cm from the video camera. Since multiple images were captured at every depth, images were averaged at each respective depth for Snellen acuity to reduce the impact of bioluminescence. The visual acuity of the average images was two times better for luxes < 0.005 or deeper than 5m. Visual acuity allowed for a direct comparison with night vision goggles (NVGs). NVGs heavily outperformed the video camera, but this was expected when comparing the underwater medium of coastal water versus air.

The study is the first of its kind for evaluating low-light video cameras. There are no other video cameras manufactured for immediate underwater use in today's market with comparable low-light sensitivities. There were also some limitations. The automatic iris and automatic dynamic range adjust the amount of light that reaches the sensor and the contrast of the overall image. Both controls are entirely automated, and though user-friendly, this may not result in the best image. It is unclear whether the impact of the bioluminescence on these controls. The bioluminescence was too much during open ocean deployments for the dynamic range to handle. However, there were moments of clarity where the bioluminescence seemingly lighted up targets to 25 m depth. If bioluminescence is located further behind the video camera, it may be a valuable light source.

The low-light underwater testing of the video camera will continue in the coming years at the Naval Postgraduate School in Monterey Bay, CA. Testing will incorporate Modulation Transfer Function (MTF) analysis associated International Organization for Standardization charts and compatible software to pinpoint the visual acuity of the video camera. The MTF analysis allows for a more accurate estimate of visual acuity, eliminating much of the potential for human error. Additional testing will also seek to adjust the frame to limit the amount of bioluminescence stirred up during harbor and open ocean deployments. It will also be essential to find a compatible open water source, such as Lake Tahoe, where the system can be deployed in a low-light environment that is both deep and clear. The setting would help identify a more precise depth or level of darkness. The system could reach and still maintain visibility without biofouling and help determine if bioluminescence has a positive or negative effect on the system.

LIST OF REFERENCES

Attebo, K., P. Mitchell, and W. Smith, 1996: Visual acuity and the causes of visual loss in Australia: The blue mountains eye study. *Ophthalmology*, **103**, 357–364, https://doi.org/10.1016/S0161-6420(96)30684-2.

Batistić, M., and Coauthors, 2012: Biological evidence of a winter convection event in the South Adriatic: A phytoplankton maximum in the aphotic zone. *Continental Shelf Research*, **44**, 57–71, https://doi.org/10.1016/j.csr.2011.01.004.

de Busserolles, F., and N. J. Marshall, 2017: Seeing in the deep-sea: visual adaptations in lanternfishes. *Phil. Trans. R. Soc. B*, **372**, 20160070, https://doi.org/10.1098/rstb.2016.0070.

Canon, 2015: Canon ME20F-SH Multi-Purpose Camera Manual. Accessed January 26 2021, https://www.usa.canon.com/internet/portal/us/home/products/details/camcorders/professional/me20f-sh

Danilenko, K. V., I. L. Plisov, A. Wirz-Justice, and M. Hébert, 2009: Human Retinal Light Sensitivity and Melatonin Rhythms Following Four Days in Near Darkness. *Chronobiology International*, **26**, 93–107, https://doi.org/10.1080/07420520802689814.

Dibner, C., U. Schibler, and U. Albrecht, 2010: The mammalian circadian timing system: organization and coordination of central and peripheral clocks. *Annu. Rev. Physiol.*, **72**, 517–549, https://doi.org/10.1146/annurev-physiol-021909-135821.

Dickey, T. D., G. W. Kattawar, and K. J. Voss, 2011: Shedding new light on light in the ocean. *Physics Today*, **64**, 44–49, https://doi.org/10.1063/1.3580492.

Howett, G. L., 1983: Size of letters required for visibility as a function of viewing distance and observer visual acuity. NBS Technical Note 1180, 76 pp, https://www.govinfo.gov/content/pkg/GOVPUBC13ff8dc22d75e66f29ebdb2bb2085ee683/pdf/GOVPUB-C13ff8dc22d75e66f29ebdb2bb2085ee683.pdf.

Huber, R., C. Nowak, B. Spatzek, and D. Schreiber, 2002: Adaptive aperture control for image acquisition. *Sixth IEEE Workshop on Applications of Computer Vision, 2002. (WACV 2002). Proceedings.*, 320–324.

Idrees, P., 2020: How the samsung galaxy S20 ultra takes great photos with nona binning. *Samsung Galaxy S20 Forum*, Accessed 01 April 2021, https://www.xda-developers.com/samsung-galaxy-s20-ultra-108mp-nona-binning-camera/.

Litwiller, D., 2001: CCD vs. CMOS: Facts and fiction. *Phonetics Spectra*, **35**, 154-158, https://courses.cs.duke.edu//cps274/compsci527/cps274/fall11/papers/Littwiller01.pdf.

Litwiller, D., 2005: CMOS vs. CCD: Maturing technologies, maturing markets. *Phonetics Spectra*, **39**, 54–59, https://www.photonics.com/Articles/CMOS_vs_CCD_Maturing_Technologies_Maturing/a22471#:~:text=CCD%20and%20CMOS%20technology&text=Integration%20and%20power%20dissipation%20are,an%20automatic%20advantage%20for%20CMOS.

MathWorks, 2021:Edge Detection methods for finding object boundaries in images. Accessed 12 April 2021, https://www.mathworks.com/discovery/edge-detection.html.

Mobley, C. D., and L. K. Sundman, 2001: Hydrolight 4.2 Technical Documentation. Accessed 04 April 2020, https://www.comm-tec.com/prods/mfgs/Sequoia/manuals/h42techdoc.pdf

Nilsson, D.-E., E. J. Warrant, S. Johnsen, R. Hanlon, and N. Shashar, 2012: A unique advantage for giant eyes in giant squid. *Current Biology*, **22**, 683–688, https://doi.org/10.1016/j.cub.2012.02.031.

Parush, A., M. S. Gauthier, L. Arseneau, and D. Tang, 2011: The human factors of night vision goggles: perceptual, cognitive, and physical factors. *Reviews of Human Factors and Ergonomics*, **7**, 238–279, https://doi.org/10.1177/1557234X11410392.

Petschnigg, G., R. Szeliski, M. Agrawala, M. Cohen, H. Hoppe, and K. Toyama, 2004: Digital photography with flash and no-flash image pairs. *ACM Trans. Graph.*, **23**, 664–672, https://doi.org/10.1145/1015706.1015777.

Pinkus, A., and H. L. Task, 1998: *Measuring observers' visual acuity through night vision goggles*. Air Force Laboratory, Accessed 22 November 2020, https://apps.dtic.mil/sti/pdfs/ADA430646.pdf.

Revell, S. J., and P. Hignett, 2004: MONIM: the new met office night illumination model. *Meteorol. Appl.*, **11**, 221–229, https://doi.org/10.1017/S1350482704001276.

Stephany, S., H. Velho, F. Ramos, and C. Mobley, 2000: Identification of inherent optical properties and bioluminescence source term in a hydrologic optics problem. *Journal of Quantitative Spectroscopy & Radiative Transfer*, **67**, 113–123, https://doi.org/10.1016/S0022-4073(99)00199-5.

Strickland, J. D. H., 1958: Solar radiation penetrating the ocean. A review of requirements, data and methods of measurement, with particular reference to photosynthetic productivity. *J. Fish. Res. Bd. Can.*, **15**, 453–493, https://doi.org/10.1139/f58-022.

Teledyne Bowtech Ltd, 2020: Teledyne Bowtech Explorer Pro Low Light Monochrome Camera, 4 pp. Accessed 08 January 2020, http://www.teledynemarine.com/explorer-pro.

Thorpe, L., 2016: Advances in CMOS image sensors and associated processing. Canon white paper CMOS, 20 pp, http://downloads.canon.com/nw/learn/white-papers/cinema-eos/White_ Paper_AdvancesinCMOS.pdf

Torres, J., and J. M. Menéndez, 2015: Optimal camera exposure for video surveillance systems by predictive control of shutter speed, aperture, and gain. *Real-Time Image and Video Processing,* **9400**, 238–251, https://doi.org/10.1117/12.2083182

Widder, E., 2002: Bioluminescence and the pelagic visual environment. *Marine and Freshwater Behaviour and Physiology*, **35**, 1–26, https://doi.org/10.1080/10236240290025581.

Yamakawa, M., S. Tsujimura, and K. Okajima, 2019: A quantitative analysis of the contribution of melanopsin to brightness perception. *Sci Rep*, **9**, 7568, https://doi.org/10.1038/s41598-019-44035-3.

THIS PAGE INTENTIONALLY LEFT BLANK

INITIAL DISTRIBUTION LIST

1. Defense Technical Information Center
   Ft. Belvoir, Virginia

2. Dudley Knox Library
   Naval Postgraduate School
   Monterey, California